Contrib Mineral Petrol (2006) 151: 20–44
DOI 10.1007/s00410-005-0043-6

ORIGINAL PAPER

Jade Star Lackey · John W. Valley · Hans J. Hinke

Deciphering the source and contamination history of peraluminous magmas using $\delta^{18}O$ of accessory minerals: examples from garnet-bearing plutons of the Sierra Nevada batholith

Received: 20 April 2005 / Accepted: 18 October 2005 / Published online: 6 December 2005

Abstract Peraluminous granitoids provide critical insight as to the amount and kinds of supracrustal material recycled in the central Sierra Nevada batholith, California. Major element concentrations indicate Sierran peraluminous granitoids are high-SiO_2 (68.9–76.9) and slightly peraluminous (average molar $Al_2O_3/(CaO + Na_2O + K_2O) = 1.06$). Both major and trace element trends mimic those of other high-silica Sierran plutons. Garnet (Grt) in the peraluminous plutons is almandine–spessartine-rich and of magmatic origin. Low grossular contents are consistent with shallow (< 4 kbar) depths of garnet crystallization. Metasediments of the Kings Sequence commonly occur as wallrocks associated with the plutons, including biotite schists that are highly peraluminous (A/CNK = 2.25) and have high whole rock (WR) $\delta^{18}O$ values (9.6–21.8‰, average = 14.5 ± 2.9‰, $n = 26$). Ultramafic wallrocks of the Kings–Kaweah ophiolite have lower average $\delta^{18}O$ (7.1 ± 1.3‰, $n = 9$). The $\delta^{18}O$(WR) of the Kings Sequence is variable from west to east. Higher $\delta^{18}O$ values occur in the west, where quartz in schists is derived from marine chert; values decrease eastward as the proportion of quartz from igneous and metamorphic sources increases. Peraluminous plutons have high $\delta^{18}O$(WR) values (9.5–13‰) consistent with supracrustal enrichment of their sources. However, relatively low initial $^{87}Sr/^{86}Sr$ values (0.705–0.708) indicate that the supracrustal component in the source of peraluminous magmas was dominantly altered ocean crust and/or greywacke. Also, plutons lack or have very low abundances (< 1% of grains) of inherited zircon (Zrc) cores. Average $\delta^{18}O$(Zrc) is 7.9‰ in peraluminous plutons, a higher value than in coeval metaluminous plutons (6–7‰). Diorites associated with peraluminous plutons also have high $\delta^{18}O$(Zrc), 7.4–8.3‰, which is consistent with the diorites being derived from a similar source. Magmatic garnet has variable $\delta^{18}O$ (6.6–10.5‰, avg. = 7.9‰) due to complex contamination and crystallization histories, evidenced by multiple garnet populations in some rocks. Comparison of $\delta^{18}O$(Zrc) and $\delta^{18}O$(Grt) commonly reveals disequilibrium, which documents evolving magma composition. Minor (5–7%) contamination by high $\delta^{18}O$ wallrocks occurred in the middle and upper crust in some cases, although low $\delta^{18}O$ wallrock may have been a contaminant in one case. Overall, oxygen isotope analysis of minerals having slow oxygen diffusion and different times of crystallization (e.g., zircon and garnet), together with detailed textural analysis, can be used to monitor assimilation in peraluminous magmas. Moreover, oxygen isotope studies are a valuable way to identify magmatic versus xenocrystic minerals in igneous rocks.

Electronic Supplementary Material Supplementary material is available for this article at http://dx.doi.org/10.1007/s00410-005-0043-6

Communicated by Jochen Hoefs

J. S. Lackey (✉) · J. W. Valley · H. J. Hinke
Department of Geology and Geophysics,
University of Wisconsin, Madison, WI 53706, USA
E-mail: jlackey@wooster.edu
Tel.: +1-330-2632297
Fax: +1-330-2632249

Present address: J. S. Lackey
Department of Geology, The College of Wooster,
Wooster, OH 44691, USA

Present address: H. J. Hinke
Malcolm Pirnie Inc, 104 Corporate Park Dr.,
White Plains, NY 10602, USA

Introduction

Peraluminous granitoids bear critical information about processes by which preexisting crust and sedimentary rocks are recycled in igneous rocks. The high aluminum content of these rocks, defined by aluminum saturation index [ASI = molar $Al_2O_3/(CaO + Na_2O + K_2O)$] values > 1.0, is often cited as evidence that peraluminous magmas contain a significant component of supracrustal

rocks, although extreme differentiation of metaluminous magmas can produce weakly peraluminous compositions as well (Clemens and Wall 1981; Zen 1988; Miller and Barton 1990; Patino-Douce and Johnston 1991; Chappell and White 1992; Chappell 1999). Strongly peraluminous (ASI > 1.1) compositions may be entirely derived from melting of crustal sources (metasedimentary rocks or high-Al continental crust).

In convergent margin batholiths, mantle and lower crustal melting leads to recycling of igneous protoliths as the dominant source of magmas. Peraluminous magmas in such settings are likely to be hybrid magmas, not generated entirely from metasedimentary sources (White et al. 1986; Patino-Douce 1999). Such peraluminous magmas may therefore provide insight to the fate of supracrustal rock in arc settings that either may be subducted beneath the arc or incorporated from above.

Estimates of the relative contribution of mantle versus preexisting crust to the magmas that formed the voluminous (> 1,000,000 km^3) Sierra Nevada batholith (SNB) remain controversial, but are critical for estimating rates of Mesozoic crustal growth. For example, some studies argue that the entire thickness of crust and sedimentary rocks above the Sierra Nevada arc was recycled in the Cretaceous (Saleeby et al. 2003), with zero net crustal growth (Ducea 2002). Low growth assumes that the isotopic composition of most SNB magmas is inherited from the overlying crust and sediments. In contrast, other studies estimate abundant crustal growth, concluding that a large part of the SNB was generated from enriched lithospheric mantle with little input from the overlying prebatholithic crust (Coleman et al. 1992; Coleman and Glazner 1997). Because the above studies in large part are based on radiogenic isotope (Sr, Nd, Pb) analyses, they are disposed to detect recycling of crust and lithospheric mantle rocks that are old enough to have measurable ingrowth of radiogenic daughter isotopes. Therefore, recycling of young (similar age to the arc) ocean crust or arc volcanic rocks in the SNB, which would increase crustal growth estimates, has not been adequately considered.

Oxygen isotopes are well-suited to resolve the contribution of mantle versus supracrustal rocks in arc settings and are excellent for detecting recycling of young ocean crust and arc volcanic rocks. Young, mantle-derived rocks erupted on or near Earth's surface are often hydrothermally altered prior to subduction, which alters $\delta^{18}O$ values; however, radiogenic isotope ratios are either only modestly reset (Sr) or are not reset (Nd, Pb). Thus, oxygen (or hydrogen) isotopes are often the only means to quantify the recycling of young ocean crust or arc plutonic and volcanic rocks in convergent margin granitoids.

Zircon (Zrc) is a common magmatic accessory mineral in peraluminous magmas, and at appropriate pressure and temperature conditions, garnet (Grt) will crystallize due to the elevated aluminum content in such magmas (Zen 1988). Slow intracrystalline oxygen diffusion in zircon (Valley et al. 1994; Watson and Cherniak 1997; Peck et al. 2003) and garnet (Coughlan 1990; Vielzeuf et al. 2005) means that $\delta^{18}O$ values of these minerals are "quenched-in" upon crystallization. Thus, garnet-bearing peraluminous magmas contain two minerals whose $\delta^{18}O$ provides a record of the high temperature processes granitoids undergo as *magmas* (King and Valley 2001; Lackey et al. 2002a; Valley 2003). Oxygen isotope ratios in most other minerals in peraluminous magmas are prone to resetting due to subsolidus recrystallization, diffusion, and hydrothermal alteration, which obscures magmatic evolution history. Valley et al. (1994, 2003) show that magmatic almandine garnet and zircon have nearly the same $\delta^{18}O$ if equilibrated. However, in the Idaho batholith, $\delta^{18}O$ values of magmatic garnet are up to 0.5‰ greater than zircon in same rock (King and Valley 2001). Thus it appears that the magmas assimilated high-$\delta^{18}O$ rocks between the time of early zircon crystallization and that of later garnet, causing $\delta^{18}O$(Grt) to be higher than $\delta^{18}O$(Zrc). Thus, garnet and zircon crystallization preserved a record of evolving magma $\delta^{18}O$.

The focus of this study is to determine if garnet and zircon from peraluminous plutons in the Sierra Nevada also contain records of ongoing magmatic contamination. Knowing the source and contamination history of Sierran peraluminous plutons can help refine estimates of crustal growth and recycling in the Sierran arc. These parameters are critical to understanding heat balance, cooling rates, and volatile budgets (e.g., H_2O, CO_2), which in turn control volcanic eruptions or processes of ore formation. Further, this study shows that oxygen isotope composition from the time of crystallization, without re-equilibration, creates a continuous record of magmatic evolution that can be used to study the crystallization history of peraluminous magmas worldwide.

Geology

Regional geology

Several garnet-bearing, peraluminous granitoids are located in the central Sierra Nevada (Figs. 1, 2, 3). The occurrence of garnet in these plutons was noted by early workers (Schuermann 1938; Ross 1958), who noted that garnet was unusual in Sierran granitoids. Subsequent studies concluded that garnet was magmatic, and not xenocrystic, based on textural characteristics and cation chemistry (Wones et al. 1969; Guy 1980; Calk and Dodge 1986; Ague and Brimhall 1988a, b; Liggett 1990; Brimhall et al. 1992).

Characteristic field, geochronologic, and geochemical data for the plutons studied are compiled in Table 1. Metamorphic wallrocks associated with the plutons, mostly from the Kings Sequence, were also sampled and studied (Figs. 1, 2, 3). Plutons were characterized using one or more zircon samples, and three of these plutons, the Tharps Peak, Dinkey Dome, and Grant Grove

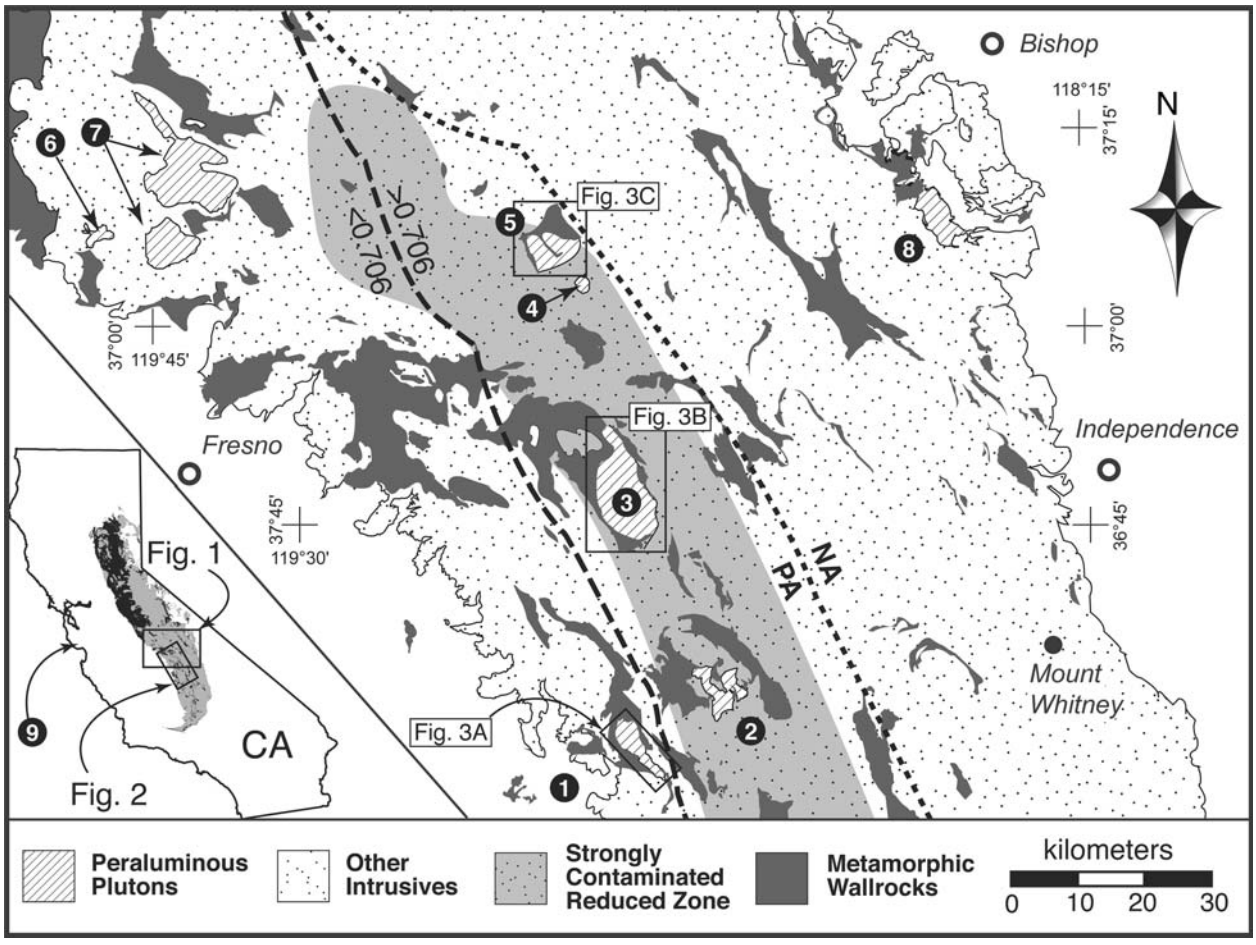

Fig. 1 Geologic map of the central Sierra Nevada showing locations peraluminous plutons studied: *1* Tharps Peak Granodiorite; *2* Cactus Point Granite; *3* Grant Grove Granite; *4* Granite of Snow Corral Meadow; *5* Dinkey Dome Granite; *6* Granite of Hensley Lake; *7* Ward Mountain Trondhjemite; *8* Rawson Creek Leucogranite. The Smith Grade Granite *9*, in the Salinian Terrane, was also studied because the pluton shares a similar geologic setting (i.e., pluton–wallrock relations, size, age) to peraluminous plutons in the Sierra Nevada. Initial $^{87}Sr/^{86}Sr = 0.706$ and 'Panthalassan' (*PA*)—'North American' lithospheric boundary are from Kistler (1990). Strongly contaminated and reduced domain after Ague and Brimhall (1988b). Map after Jennings et al. (1977), Moore and Sisson (1987), and Bateman (1992)

(Fig. 3) were studied in detail. Most plutons studied are small (< 150 km^2; Table 1). They often lack magmatic foliation, and intruded later than surrounding metaluminous plutons (Bateman 1992), and all but one are Cretaceous (Table 1). Several plutons are in direct contact with sizeable (1–5 km^2) mafic (gabbro-diorite) bodies that are undated (Table 1), though field relations, such as inclusion within the peraluminous plutons, suggest they are coeval. Initial $^{87}Sr/^{86}Sr$ (Sr_i) values of the peraluminous plutons range from 0.704 to 0.708, and thus do not exceed the > 0.710 Sr_i boundary that Chappell and White (1992) considered to mark true S-type granites. Most plutons occur in parts of the batholith thought to be underlain by "oceanic" lithosphere, i.e., west of Kistler's (1990) boundary dividing the accreted oceanic terranes (Panthalassan lithosphere) of the western SNB and continental crust (North American lithosphere) in the eastern SNB (Figs. 1, 2). Several of the plutons are in the strongly contaminated and reduced domain of the batholith (Fig. 1), where the melting of graphite-rich metasedimentary rocks leads to magmas being relatively reduced (0–2 log fO_2 units below QFM, Ague and Brimhall 1988a, b). Ilmenite, instead of magnetite + titanite, is found in the reduced plutons. The Rawson Creek leucogranite (Fig. 1) is an eastern Sierra pluton with similar mineral assemblage, and association with graphitic wallrocks, as occurs in western strongly contaminated and reduced plutons (Hathaway 1996).

This study also presents findings for the Cretaceous garnet-bearing Smith Grade Granite (Table 1). The Smith Grade Granite occurs ~200 km west of the Sierra Nevada, in the Salinian Terrane (Fig. 1), which is displaced and its original Cretaceous position in either the eastern Sierra or farther south in the Cordillera (cf. Schott et al. 2004). The Smith Grade Granite is included in the study because it shares a comparable Cretaceous magmatic arc setting with peraluminous plutons in the Sierra Nevada.

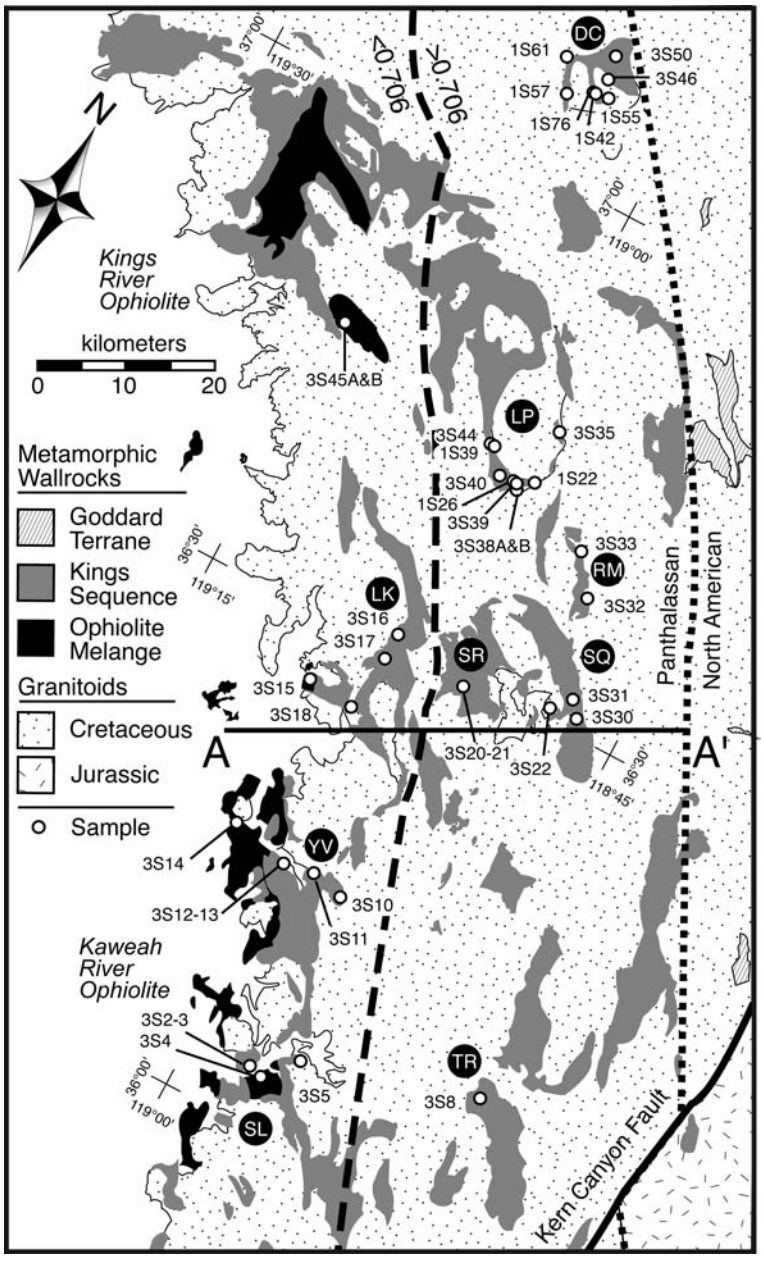

Fig. 2 Map showing locations of metamorphic wallrock samples. *Transect line* (*A–A′*) is used in Fig. 8 to show regional $\delta^{18}O$(WR) pattern of the Kings Sequence. Pendant abbreviations: *DC* Dinkey Creek; *LK* Lake Kaweah; *LP* Logger Point; *RM* Redwood Mt.; *SL* Success Lake; *SQ* Sequoia; *SR* Sheep Ridge; *TR* Tule River; *YV* Yokol Valley. Map references as in Fig. 1

Metamorphic wallrocks of the Kings Sequence occur throughout the central Sierra Nevada. The Kings Sequence is dominantly biotite schists of Triassic–Jurassic age (Fig. 2). Wallrocks occur as highly deformed, steeply dipping screens between plutons with concordant foliations having strong to moderate down-dip constrictional fabrics (Saleeby and Busby 1993). During emplacement of adjacent granitoids, Kings Sequence screens were heated and behaved in a ductile manner, which allowed the screens to be drawn downward as a consequence of *syn*-magmatic "return flow" (Saleeby 1990).

The peraluminous character of the strongly contaminated and reduced plutons appears linked to assimilation of Kings Sequence schists. However, much of the assimilation likely occurred at depth, below the present levels of exposure, because a number of the strongly contaminated and reduced plutons lack such high-Al metasedimentary rocks at their margins. On the other hand, a number of the strongly contaminated and reduced plutons are intimately associated with the Kings Sequence. The distribution of garnet and other peraluminous index minerals (muscovite, andalusite, sillimanite, spinel) may be localized near metasedimentary wallrocks at the margins of some plutons (e.g., Fig. 3c).

Pluton–wallrocks contacts

There are well-exposed contacts of peraluminous plutons with adjacent metasedimentary wallrocks. Pluton–

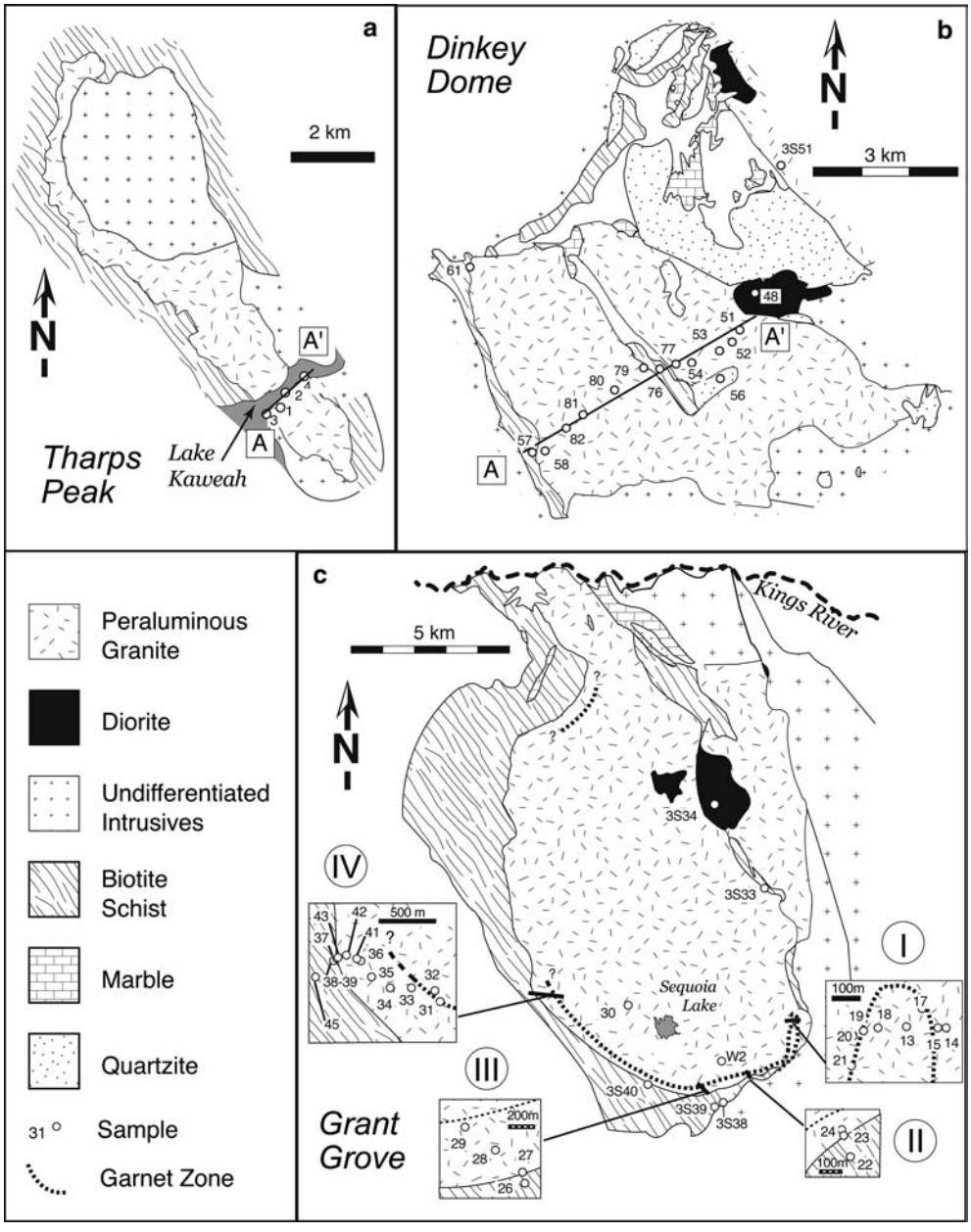

Fig. 3 Geology and sample location maps of the **a** Tharps Peak, **b** Dinkey Dome, and **c** Grant Grove plutons. Garnet is pervasive in the Tharps Peak and Dinkey Dome plutons, whereas a discrete garnet zone is mapped in the margin of the Grant Grove pluton. Note: all samples have the prefix"1S" unless otherwise noted. Samples in the Tharps Peak and Dinkey Dome plutons are projected onto the transect line A–A′. Sampling Transects I–IV in the Grant Grove pluton are indicated with *heavy lines*. For simplification, adjacent intrusives are undifferentiated. Maps after **a** Liggett (1990); **b** Bateman and Wones (1972); **c** Moore and Sisson (1987) and J.G. Moore (unpublished mapping)

wallrock contacts are often sharp (Fig. 4a), and show little evidence for stoping or other physical disaggregation of the wallrocks. Generally, there is limited evidence for melting of wallrock. The central wallrock screen bisecting the Dinkey Dome pluton (Fig. 3b) displays localized (1 m from contact) anatexis of the mica schist by the granite, which is manifested as leucocratic segregations (Fig. 4b). Xenoliths of wallrock were observed near the eastern margin of the Tharps Peak pluton; some xenoliths exhibit partial melting textures (Fig. 4c). Pegmatite and aplite dikes within the plutons were noted both near and far from contacts; these are late stage and auto-intrusive. Dikes intruding from plutons into metasedimentary wallrock are rare. Peraluminous plutons abut and occasionally include (e.g., Grant Grove) diorites, though contacts are poorly exposed. We note that igneous mafic enclaves are occasionally observed in the peraluminous plutons, but are not nearly as abundant or common as in metaluminous plutons.

Petrography

Granitoids

The plutons studied typically contain magmatic quartz, K-feldspar (perthitic), plagioclase (Ab_{88-97} in the Grant Grove pluton; see Supplementary Data Table), and biotite, with accessory muscovite, garnet, zircon, apatite, and monazite (Table 1).

Table 1 Summary geologic, geochronologic, isotopic, and mineralogic data for Sierra Nevada peraluminous plutons

Pluton/unit	Map no.	Area (km^2)	Age (Ma)	Initial $^{87}Sr/^{86}Sr$	Metamorphic wallrocks	Mafic bodies	Garnet location	No. of garnet types	Accessory minerals	Other
Tharps Peak Granodiorite	1	10.5	109.5[d]	0.7049[d]	Mica Schist	No	Ubiquitous	2	Mu, Mzt	
Cactus Point Granite	2	26.2	< 99[a]	0.70610[j]	Mica Schist, Marble	Yes	Unknown	2	Mu	
Grant Grove Granite	3	106.3	98[j] 106[a]	0.70530[e] 0.70818[e]	Mica Schist, Marble, Quartzite	Yes	Margin Facies	2	And, Au, Ghn, Grph, Mgt, Mu, Mzt, Rut, Sill, Ttn2	Feldspars altered
Granite of Snow Corral Meadow	4	4.7	90[c]	–	None	No	Ubiquitous	1	Mzt, Ttn1, Ttn2	
Dinkey Dome Granite	5	30.3	90[c]	0.7065[g]	Quartzite, Mica Schist, Calc-Silicate	Yes	Ubiquitous	2	And, Moly, Mu, Sill, Urn	
Granodiorite of Hensley Lake	6	9.4	116[c]	–	None exposed	No	Ubiquitous	1	Mu, Sill	
Ward Mountain Trondhjemite	7	150.7	115[b]	0.70444[g] 0.70478[f]	None exposed	Yes	Unknown	1	Mu, Mzt	
Rawson Creek Leucogranite	8	11.3	165[j]	–	Mica Schist	Yes	Unknown	3	Mu, Pyr, Ttn2	Feldspar and micas altered
Smith Grade Granite	9	8.7	111[h]	0.70565[i]	Mica Schist, Marble	Yes	Ubiquitous	2	Moly, Mu	

Major minerals in plutons studied include: Quartz, K-feldspar, Plagioclase, Biotite. "Mafic Bodies" indicates any gabbro/diorite bodies are in direct contact with a peraluminous pluton. Metamorphic wallrocks listed in order of decreasing abundance
And andalusite; *Au* elemental gold; *Ghn* gahnite; *Grph* graphite; *Mgt* magnetite; *Moly* molybdenite; *Mu* muscovite; *Mzt* monazite; *Pyr* pyrite; *Rut* rutile; *Sill* sillimanite; *Ttn* titanite (*1* primary; *2* secondary); *Urn* urananite

[a]Chen and Moore 1982
[b]Stern et al. 1981
[c]Bateman 1992
[d]Liggett 1990
[e]Chen and Tilton 1991
[f]Truschel 1996
[g]R.W. Kistler, written communication
[h]James 1992
[i]Kistler and Champion 2001
[j]Wenner and Coleman 2003

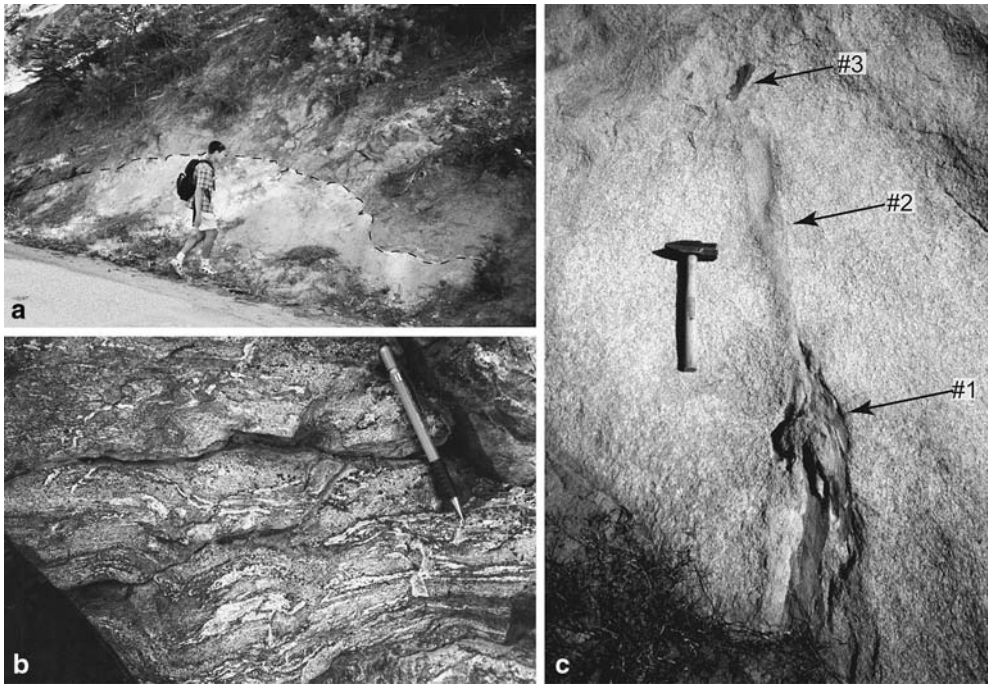

Fig. 4 Field relations. **a** A sharp pluton (*light*)–wallrock (*dark*) contact exposed on Hwy 180 in the Grant Grove pluton. **b** Partial melting and leucosome development in biotite–schist 5 m from the Dinkey Dome pluton. Pencil for scale is 16 cm long. **c** Metasedimentary xenoliths in the Tharps Peak pluton. Lower xenolith (*1*) is well defined but grades into a diffuse leucocratic zone (*2*). A smaller, well-defined xenolith (*3*) is visible in the background. Hammer handle is 27 cm long

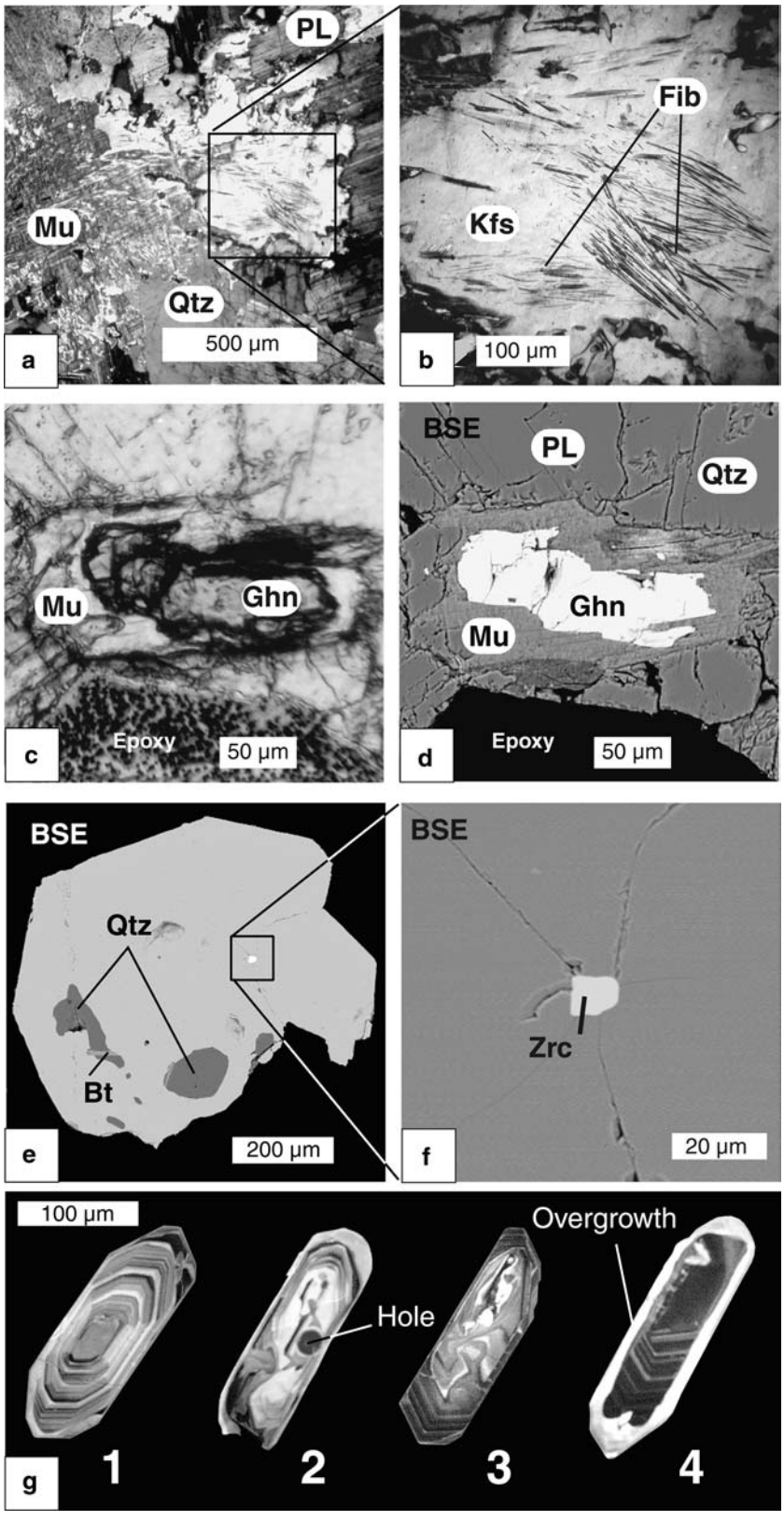

Fig. 5 Petrographic textures. **a, b** Reaction (1) of muscovite (*Mu*) + quartz (*Qtz*) to K-feldspar (*Kfs*) and fibrolitic sillimanite (*Fib*) is evident in some samples as a late replacement texture (1S36). **c, d** A muscovite corona on gahnite-rich spinel in the Grant Grove pluton in plane polarized light (**c**) and BSE (**d**); (1S37). **e, f** Garnet phenocryst containing inclusions of quartz, biotite (1S18). Zircon inclusions indicate some zircon crystallized before garnet. **g** Cathodoluminescence imaging of zircon reveals normal oscillatory zonation (*1* 1S30), convolute zonation (*2* 1S67; *3* 1S79), and an example of an inherited core (*4* 1S4)

A number of less common magmatic accessory minerals were also identified. The Grant Grove pluton (Fig. 3c) contains a discontinuous garnet zone at its outer margin (Fig. 3c) that contains a diverse assemblage of other accessory minerals. Sillimanite was previously reported in the garnet zone of the Grant Grove pluton (Chen and Moore 1982), and was identified in eight samples, sometimes coexisting with fibrolite. Silli-

manite occurs in complex intergrowths with K-feldspar and is associated with late breakdown of magmatic muscovite (Fig. 5a, b) by Reaction (1):

$$\text{muscovite} + \text{quartz} = \text{sillimanite} + \text{K-feldspar} + H_2O \pm \text{melt}. \quad (1)$$

Reaction 1 may have resulted due to decompression or an increase of water activity in the magma. Alternatively, a temperature increase (possibly due to intrusion of a magma nearby) could have caused the breakdown of muscovite. The garnet zone of the Grant Grove pluton also contains accessory andalusite ($n = 1$ sample), rutile ($n = 3$), graphite ($n = 5$), elemental gold ($n = 1$), and gahnite–hercynite spinel [$(Zn_{(0.51\text{-}0.66)}Fe_{(0.48\text{-}0.31)}\ Mg_{(0.01\text{-}0.03)})Al_2O_4$] ($n = 5$), which is previously unreported in the SNB. The gahnite-rich spinel crystallized early and only occurs as inclusions within garnet or surrounded by coronas of muscovite (Sample 1S37, Fig. 5c, d). The occurrence of spinel in five samples from the western part of the pluton defines a narrow "spinel" zone that extends 100–200 m into the pluton; notably, the interior of the pluton contains magnetite.

The Dinkey Dome pluton (Fig. 3b), which contains garnet throughout (Table 1), also has distinct mineralogy. The east side of the pluton contains andalusite and sillimanite (Guy 1980; Hinke 2002, Hinke et al. 2002), coexisting in some cases. Hinke (2002) reports abundant monazite throughout the pluton and molybdenite and uraninite in the east side of the pluton. The reducing conditions in the Dinkey Dome pluton (2 log fO_2 units below QFM; Guy and Wones 1980) permitted uraninite crystallization. The only other reported occurrence of magmatic uraninite in the Sierra is from a single locality in the Bass Lake tonalite (Snetsinger and Polkowski 1977).

Garnet was studied in detail to confirm magmatic crystallization. Abundance of garnet varies considerably, although it is usually less than 0.5 modal%. Garnet phenocrysts are euhedral to subhedral, and rarely exceed 1 mm in diameter. Several plutons have two populations of garnet (Table 1), which are recognized by differences in garnet color, as well as slight shifts of chemistry (see Garnet chemistry discussion). For instance, two populations of garnet (pale pink and dark red) were identified in the Grant Grove and Dinkey Dome plutons. Generally, garnets contain very few inclusions, which is consistent with magmatic origin (Allan and Clarke 1981). In some cases zircon is included in garnet (Fig. 5e, f) in samples from the Grant Grove and Dinkey Dome plutons, showing that some zircon grew before garnet in these plutons, but this does not indicate that all zircon crystallized before garnet. Sillimanite occurs as inclusions in the cores of garnets from the Hensley Lake granite.

We note that garnet in some Sierran granitoids may have crystallized under near- or subsolidus conditions, especially in aplites, and thus be of hydrothermal and/or metamorphic origins. Simple reheating of older plutons by younger ones may cause some in situ garnet crystallization. Because they would not directly be of igneous origin, such garnets would exhibit disequilibrium $\delta^{18}O$ fractions when compared to primary magmatic minerals. Oxygen isotope data presented later in the paper suggest that in some cases garnet did crystallize at subsolidus temperatures.

Cathodoluminescence imaging of zircon crystals was used to document the internal growth structure of zircons and to screen for inherited cores. Crystals from the peraluminous plutons commonly display oscillatory growth zonation (Fig. 5g, no. 1). Zircon in some samples displays convolute internal structure (Fig. 5g, nos. 2, 3), possibly a result of radiation damage (see Corfu et al. 2003). Zircon crystals from two plutons, Tharps Peak and Snow Corral Meadow, have inherited cores that display oscillatory zonation; these cored grains have overgrowths that also display oscillatory zonation (e.g., Fig. 5g, no. 4). A cathodoluminsecence survey of over 100 zircons each from the Tharps Peak and Snow Corral Meadow plutons indicates that $< 1\%$ of the grains contain cores (B. Fu et al., unpublished data). It is notable that despite the peraluminous nature of the plutons studied, there is a general lack or low abundance of inherited zircons.

Metamorphic wallrocks

Schists of the Kings Sequence were studied to understand the distribution of metamorphic garnet in the study area. Typically, samples are spotted hornfels containing biotite + quartz ± K-feldspar ± andalusite ± sillimanite ± cordierite (Lackey 2005), and of the 26 schists analyzed, only 1 (3S12) contains metamorphic garnet. Garnet in this rock was poikioblastic and sub- to anhedral, and does not resemble the magmatic garnets studied. Evidently, peak metamorphic conditions (2–3 kbar, 550–625°C), as well as the high Mg content of Kings Sequence, were unfavorable for crystallization of metamorphic garnet (Lackey 2005).

Analytical techniques

Forty-seven samples were collected from peraluminous plutons and three from associated diorites. Zircon was separated from 36 of these samples. Additionally, metamorphic wallrocks ($n = 37$) were studied petrographically and analyzed for whole rock $\delta^{18}O$ for comparison with the granitoids. Selected samples ($n = 31$) were analyzed for major and five trace elements by X-ray fluorescence at XRAL Laboratories, Canada (Table 2).

Zircon and garnet were separated from 5 to 20 kg samples by standard crushing, density, and magnetic separation techniques. Sulfides and phosphates were dissolved from zircon concentrates with hot (~85°C), concentrated nitric acid, after which the concentrates

Table 2 Major and trace element compositions of peraluminous granitoids and selected wallrocks in the central Sierra Nevada

	Granitoids																			
Sample	1S1	1S2	1S3	1S4	1S5	1S23	1S24	1S27	1S28	1S29	1S30	1S51	1S52	1S53	1S54	1S58	1S67	1S77	1S79	1S80
SiO_2	73.4	73.5	72.8	72.0	73.6	74.7	73.4	75.6	76.4	75.9	68.9	76.7	76.0	76.4	75.6	75.0	75.6	76.9	73.4	74.5
Al_2O_3	14.3	14.5	14.5	14.8	13.9	14.3	14.1	14.3	14.0	14.2	16.7	13.2	13.7	13.5	13.9	13.5	13.2	13.2	14.3	13.8
CaO	1.84	2.09	1.51	2.10	1.63	0.69	0.64	0.16	0.27	0.37	1.56	0.40	0.25	0.37	0.38	1.22	1.49	0.43	1.78	1.36
MgO	0.40	0.42	0.38	0.48	0.46	0.15	0.12	0.07	0.07	0.09	0.61	0.13	0.12	0.11	0.11	0.34	0.37	0.13	0.45	0.39
Na_2O	4.33	4.21	4.07	4.27	3.49	3.73	3.44	1.95	3.21	3.35	3.58	3.78	3.74	3.82	3.67	3.46	2.67	3.82	3.85	3.58
K_2O	2.70	2.64	3.44	2.97	3.61	5.08	5.26	5.48	4.67	4.69	5.47	4.34	4.36	4.30	4.42	3.93	4.90	3.91	3.55	3.96
Fe_2O_3	1.88	2.04	1.99	2.06	2.51	1.00	0.58	0.53	0.66	0.61	2.26	1.15	1.38	1.22	1.35	1.79	1.42	1.34	2.28	2.01
MnO	0.05	0.06	0.03	0.07	0.06	0.03	0.02	0.04	0.02	0.05	0.06	0.07	0.09	0.08	0.08	0.08	0.02	0.08	0.07	0.06
TiO_2	0.13	0.15	0.12	0.16	0.23	0.06	0.04	0.02	0.03	0.02	0.26	0.03	0.04	0.03	0.03	0.15	0.19	0.02	0.21	0.18
P_2O_5	0.05	0.06	0.03	0.05	0.12	0.01	0.02	0.02	<0.01	0.02	0.07	0.04	0.04	0.04	0.04	0.04	0.02	0.03	0.07	0.07
LOI	0.50	0.30	0.30	0.35	0.45	0.25	0.45	1.85	0.95	0.80	0.75	0.40	0.60	0.35	0.65	0.70	0.30	0.40	0.35	0.25
Total	99.58	99.97	99.17	99.31	100.06	100.00	98.07	100.02	100.28	100.10	100.22	100.24	100.32	100.22	100.23	100.21	100.18	100.26	100.31	100.16
Rb	82	73	76	71	140	111	107	172	140	142	138	213	248	226	224	179	113	199	174	208
Sr	157	184	148	188	148	83	69	14	11	12	261	22	25	19	18	124	225	19	172	134
Ba	980	982	1,910	1,120	1,020	709	603	151	103	114	1,400	134	158	115	121	383	1,080	102	501	461
Y	25	25	32	30	31	17	15	45	42	31	19	35	46	37	38	47	14	37	31	33
Zr	89	95	94	88	165	93	71	57	94	55	119	60	59	59	51	116	121	50	139	119
Nb	10	11	10	8	14	10	10	11	12	11	14	23	33	26	24	21	8	20	25	25
A/CNK	1.02	1.02	1.04	1.01	1.04	1.02	1.03	1.34	1.18	1.15	1.05	1.05	1.11	1.07	1.11	1.04	0.98	1.09	1.01	1.02
Mg no.	29.6	29.0	27.4	31.6	26.6	22.9	29.1	20.7	17.4	22.6	34.8	18.3	14.7	15.1	13.9	27.3	34.0	16.1	28.1	27.8
Zrc Sat. (°C)	740	745	747	736	797	748	728	735	765	719	764	719	722	719	710	768	768	708	777	768

were soaked in cold (25°C), concentrated hydrofluoric acid (12–15 h) according the method of King and Valley (2001). Hydrofluoric acid preferentially dissolves radiation-damaged material from zircons, which is subject to alteration of $\delta^{18}O$ (Valley 2003). A final cleaning of zircons in hot (~85°C), concentrated hydrochloric acid (30 min) removes any residual fluorides. Final sample purification was done by hand picking under a binocular microscope. Zircon grains were powdered for oxygen isotope analysis with a boron-carbide mortar and pestle, which limits grain-size effects and maximizes fluorination efficiency.

Mineral separates and whole rock powders were analyzed in the University of Wisconsin Stable Isotope Laboratory by laser fluorination using BrF_5 as a reagent. Isotope ratios were measured on a dual inlet gas source Finnigan MAT 251 mass spectrometer. Whole rock powders (~2 mg) were analyzed with an airlock sample chamber (Spicuzza et al. 1998a). Oxygen was liberated from silicates with BrF5 using a 30 W CO_2 laser ($\lambda = 10.6$ μm), then purified cryogenically, passed through hot Hg (to remove F_2), and finally converted to CO_2 with a hot carbon rod (Valley et al. 1995). All analyses were standardized daily by four or more analyses of UWG-2, Gore Mountain garnet standard, and sample $\delta^{18}O$ values were corrected to the long-term accepted value of 5.80‰ VSMOW for UWG-2. The average raw $\delta^{18}O$ of UWG-2 for 23 days of analyses ($n = 117$) is 5.68 ± 0.09‰ (1 SD; standard error ($1\sigma = 1SD/(n^2)$ is ± 0.008‰). Average day-to-day precision of UWG-2 is ± 0.05‰; daily corrections average 0.12‰. Average $\delta^{18}O$ of NBS-28 is 9.42 ± 0.10‰ after correction, $n = 12$, and Δ(NBS-28–UWG-2) averaged 3.68 ± 0.03‰, in excellent agreement with the UW lab long-term Δ(NBS-28–UWG-2) of 3.70 ± 0.06‰ (1 SD). During 7 days of WR analyses using the airlock chamber, raw values of UWG-2 averaged 5.66 ± 0.12‰ ($n = 33$); replicate analyses of whole rock powders averaged ± 0.14‰. Replicate analyses average better than ± 0.09‰ for quartz, by the rapid heating, defocused beam technique (Spicuzza et al. 1998b), ± 0.07‰ for garnet and ± 0.04‰ for zircon. To determine if various mineral pairs are in oxygen isotope equilibrium, intermineral fractionations [$\Delta^{18}O$(mineral-i − mineral-j)] are compared to published equilibrium fractionation factors throughout the text (Appendix 1).

Garnet compositions were measured with the University of Wisconsin CAMECA SX50 electron microprobe (see Supplementary Data Table). Analyses of cores and rims of 5–7 garnets were averaged for each sample. Analytical conditions were 15 KeV accelerating voltage and 20 nA beam current. Counting times were 10 s on peak, 10 s on background. Chemical compositions were determined with wavelength dispersive spectrometry using crystalline standards.

Major and trace element geochemistry

Major and trace element compositions were determined for representative metamorphic wallrocks and granitoids (Table 2). Major element variation diagrams for selected oxides in peraluminous granitoid samples are plotted in Fig. 6, and compared to 550 published analyses of Cretaceous plutonic rocks from the central SNB that are compiled in Lackey (2005).

Biotite schist wallrocks are highly variable in both their major and trace element compositions. They have a wide range of concentrations of most major oxides (e.g., $SiO_2 =$ 51.7–85.5; $Al_2O_3 = 7.0$–33.2; $Fe_2O_3 = 2.6$–9.8); they are highly peraluminous with A/CNK = 1.1–3.5.

									Diorites		Wallrocks									
1S81	1S82	3S51	1S92	1S93	1S95	1S96	1S128	1SG4	3S34	3S48	1S22	1S26	1S39	1S57	1S76	3S10	3S12	3S17	3S22	3S30
72.7	73.4	74.19	74.8	69.4	73.9	72.1	76.5	75.2	52.46	52.04	55.0	85.5	80.58	51.4	51.7	74.93	64.32	70.36	56.7	58.75
14.4	13.9	13.69	14.51	16.41	14.6	15.7	13.1	13.8	18.58	17.26	20.2	7.02	9.39	11.2	33.2	11.4	16.5	14.16	22.64	23.85
1.33	1.32	1.49	1.19	3.71	1.62	2.48	0.30	0.73	7.72	8.07	0.04	0.46	0.43	18.30	0.96	1.22	1.11	0.51	1.42	0.44
0.39	0.38	0.17	0.29	0.80	0.35	0.52	0.16	0.20	4.08	5.2	3.17	0.83	1.49	4.84	1.03	2.17	2.61	2.67	1.65	1.8
3.58	3.55	3.6	3.70	4.57	3.95	4.37	3.35	3.67	2.97	1.84	0.25	0.89	0.46	0.20	2.19	2.07	2.7	0.79	2.5	0.81
4.25	4.11	4.11	3.53	1.16	3.58	2.61	5.19	5.01	1.91	1.35	6.68	0.92	0.89	0.08	3.79	3.45	3.73	3.85	5.92	3.89
1.94	1.93	2.35	1.11	2.48	1.05	1.57	0.75	0.93	9.72	11.9	9.75	2.61	3.42	11.70	4.95	3.42	6.15	4.13	6.69	5.88
0.06	0.05	0.05	0.03	0.04	0.02	0.04	0.08	0.04	0.15	0.14	0.26	0.04	0.04	0.67	0.10	0.05	0.16	0.06	0.08	0.06
0.20	0.18	0.2	0.11	0.34	0.14	0.20	0.07	0.10	1.26	1.13	1.26	0.41	0.59	0.54	1.32	0.53	0.78	0.77	0.84	0.85
0.06	0.07	0.03	0.06	0.12	0.06	0.08	0.05	0.01	0.26	0.32	0.04	0.02	0.05	0.19	0.08	0.04	0.09	0.02	0.1	0.08
0.25	0.50	0.3	0.95	0.75	0.40	0.35	0.50	0.30	0.65	0.8	3.30	1.45	2.10	<0.01	0.50	0.6	2.1	2.3	1.25	2.95
99.16	99.39	100.18	100.32	99.82	99.67	100.02	100.05	99.99	99.76	100.05	99.95	100.15	99.44	99.12	99.82	99.88	100.25	99.62	99.79	99.36
206	194	140	77	36	92	71	201	141	55	53	273	47	31	4	95	106	145	111	157	174
134	136	211	146	493	251	368	51	65	498	601	13	56	61	507	244	135	94	85	151	211
509	440	1,220	865	502	962	909	304	353	904	329	2,030	213	389	46	744	1,870	1,410	2,510	1,250	2,140
36	35	58	17	10	14	12	36	38	29	12	29	20	22	36	17	41	59	43	62	36
117	124	278	54	101	75	86	60	88	148	85	236	310	366	86	273	162	275	216	189	125
25	26	19	8	5	9	8	26	12	12	6	23	11	10	9	27	13	16	14	19	17
1.04	1.02	0.98	1.13	1.04	1.03	1.04	1.02	0.99	0.87	0.89	2.20	2.01	3.48	0.33	3.23	1.13	1.46	1.95	1.57	3.31
28.5	28.0	12.5	34.1	39.0	39.8	39.6	29.7	29.9	45.4	46.4	39.2	38.6	46.3	45.0	29.2	55.7	45.7	56.1	32.8	37.7
767	771	839	713	743	729	736	718	742	728	693	–	–	–	–	–	–	–	–	–	–

Major, minor, and trace element (e.g., Al_2O_3, MnO, Rb, Sr, Y, Zr) concentrations of peraluminous plutons and associated diorites lie within the major element differentiation trends defined by other Sierra Nevada samples, including high-silica samples (Fig. 6). All but two high-silica samples are weakly peraluminous with A/CNK values of 0.98–1.34 (Fig. 6). Manganese, which can expand the stability P–T field of garnet in granitoids (Miller and Stoddard 1981), shows increasing concentrations with increasing SiO_2 in both peraluminous and metaluminous rocks. When Mn is considered with respect to Fe and Mg, as molar MnO/(FeO + MgO +

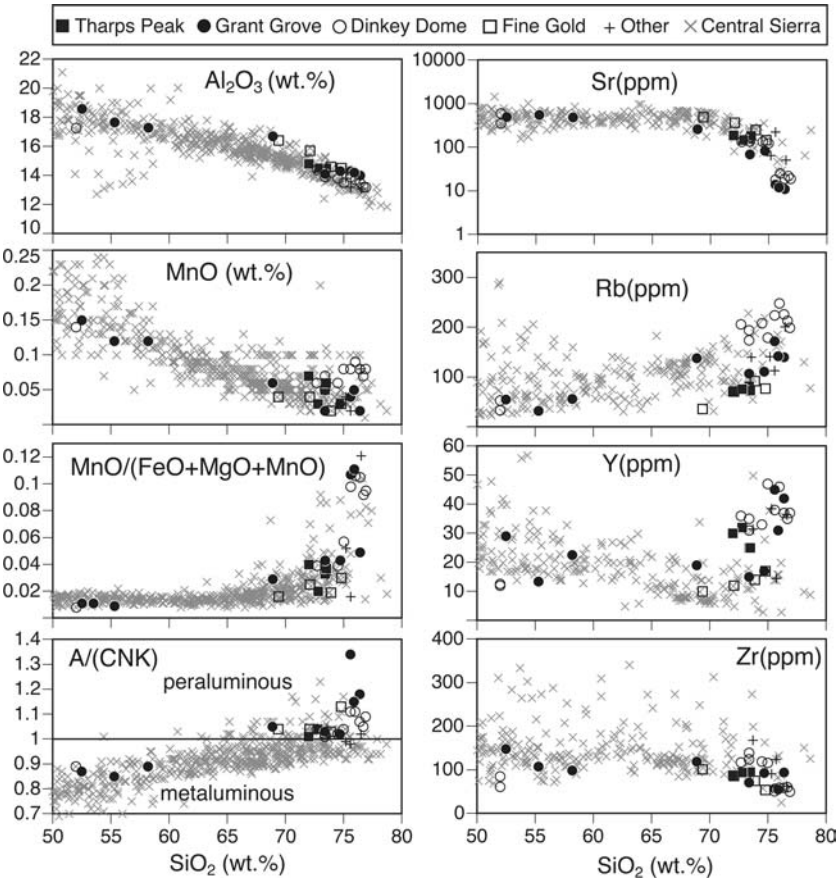

Fig. 6 Major and trace element variation diagrams for peraluminous plutons. Representative analyses of metaluminous "Central Sierra" plutonic rocks are shown for comparison. Ratios of MnO/(FeO + MgO + MnO) and Al_2O_3/(CaO + Na_2O + K_2O), A/CNK, are in molar abundance. Fine Gold intrusive suite plutons include the Granite of Hensley Lake and Ward Mt. Trondhjemite. "Other" is remaining peraluminous plutons (Table 1). Two data points for low-SiO_2 diorites are from Goldstein (2004) and Wenner and Coleman (2004)

MnO), samples from the east side of the Dinkey Dome pluton, plus some from the Grant Grove and Rawson Creek plutons, have considerably higher values than in other high-silica rocks (Fig. 6).

Trace element concentrations are highly variable from pluton to pluton, although the trends of most mimic those in metaluminous plutons. Peraluminous granitoids display depletion and enrichment of Sr and Rb, respectively, relative to low SiO_2 metaluminous plutons (Fig. 6). Yttrium concentrations deviate from patterns in metaluminous rocks, with higher Y in peraluminous plutons. Enrichment of Y has been documented in other peraluminous granites (Chappell and White 1992; Abdel 2001), although such enrichment is cited as evidence of extreme differentiation of a metaluminous to peraluminous magma, rather than a magma source characteristic (Chappell 1999).

Average Zr concentrations are relatively low (89 ± 30 ppm), except sample 1S51 (Table 2), and for a given SiO_2, most samples lie at the lower limit of Zr concentrations observed in other SNB plutons. Zircon saturation temperatures (Watson and Harrison 1983) average 743 ± 46°C (2 SD; Table 2), and suggest that zircon in the peraluminous plutons studied began to crystallize within a fairly restricted range of temperature. Saturation temperatures may overestimate the actual temperature at which zircon crystallization began if there is abundant inherited zircon (Miller et al. 2003), although only the Tharps Peak and Snow Corral Meadow plutons contain significant inheritance. In addition, because differences in intermineral fractionation are small at high temperature (Appendix 1), variable zircon saturation temperature yields minor changes of intermineral fractionations: ΔGrt–Zrc varies 0.01‰ from 789 to 697°C. Thus, differing temperatures of zircon crystallization do not significantly shift $\delta^{18}O$.

Garnet chemistry

Chemical composition is widely to determine if garnet in igneous rocks is magmatic in origin. In Sierra Nevada peraluminous plutons, garnet composition varies considerably, but can be broadly characterized as almandine–spessartine-rich ($X_{alm} = 0.39$–0.87; $X_{sps} = 0.09$–0.55), with minor pyrope ($X_{pyp} = 0.01$–0.1) and grossular ($X_{grs} = 0.01$–0.04) components (Fig. 7a, and see Supplementary Data Table). Compositions fall in the field for magmatic garnet compiled by Miller and Stoddard (1981) and are similar to compositions previously reported for granitoids in the SNB (Guy and Wones 1980; Calk and Dodge 1986; Ague and Brimhall 1988b; Liggett 1990). Zoning is subdued to nonexistent in most garnets (Profile I; Fig. 7b), but some have subtle reverse (high-Mn rims) zoning (Profile II, Fig. 7b). The most pronounced zoning of any sample is a complex "bell" shaped profile from a garnet on the east side of the Dinkey Dome pluton (Profile IV; Fig. 7b). In the Grant Grove pluton Mn is reversely zoned in pink, but normally zoned in red garnet (Profiles V and VI, Fig. 7b).

Differences in garnet chemistry in the Dinkey Dome and Grant Grove plutons correlate to the garnet color and location in the pluton. At Dinkey Dome, garnet in the west side of the pluton (Fig. 3b) has systematically higher X_{sps} and X_{pyp} content relative to the east side (Fig. 7, Profile II, vs. III and IV). Values of X_{grs} are also elevated, suggesting slightly higher pressures of crystallization on the west side. Additionally, lighter colored "pink" garnets from the east side of the pluton have consistently higher X_{sps} content (Fig. 7a). At Grant Grove, garnet nearest to wallrocks has the maximum Fe, and where pink and red garnet coexists, pink ones nearly always has higher Fe and lower Ca. The lower X_{grs} of pink garnets is consistent with crystallization at lower pressure than red garnet.

Oxygen isotope ratios

Metamorphic wallrocks

Kings sequence metasedimentary rocks

A wide range of $\delta^{18}O$ occurs in Kings Sequence rocks in the west-central SNB (Table 3). The range in $\delta^{18}O$(WR) values in biotite schists is 9.6–21.8‰ and averages 14.5 ± 2.9‰ ($n = 26$). Two schists from the Redwood Mt. Pendant (Figs. 2, 8a) were omitted from the average. Their abnormally low $\delta^{18}O$ values (6.3–6.6‰) and high modal abundance of chlorite and zoisite are uncommon for Kings Sequence schists and indicate these rocks were hydrothermally altered. Two Kings Sequence quartzite samples from the Dinkey Creek pendant have relatively low $\delta^{18}O$ values (13.0, 13.6‰, Table 3). Broadly, the range of values in the central SNB overlaps $\delta^{18}O$ values for the Kings Sequence in the southern Sierra (Ross 1983; Saleeby et al. 1987), but is lower on average. West-to-east variation in the $\delta^{18}O$ of the Kings Sequence is notable (Fig. 8b). Additionally, garnet from the sole garnet-bearing schist (3S12), has a $\delta^{18}O$ of 16.8‰, a value much higher than any magmatic garnet. In two schists in the Dinkey Creek pendant, $\delta^{18}O$(andalusite) = 9.6–11.3‰, and is 0.4–1‰ lower than $\delta^{18}O$(WR); sillimanite that overgrows andalusite has a similar $\delta^{18}O$ (Table 3).

Kings–Kaweah ophiolitic rocks

A suite of ten samples from the Kings–Kaweah ophiolite melange (Saleeby and Busby 1993), which forms the foothills of the western Sierra (Fig. 2), was analyzed for $\delta^{18}O$ (Table 3). They are representative of the upper parts of oceanic crust and include fragments of pillow basalt, serpentinite, quartzite, and a rodingite. Two gabbros intruding the ophiolite package were also analyzed. This suite has an average $\delta^{18}O$(WR) of 7.1 ± 1.3‰

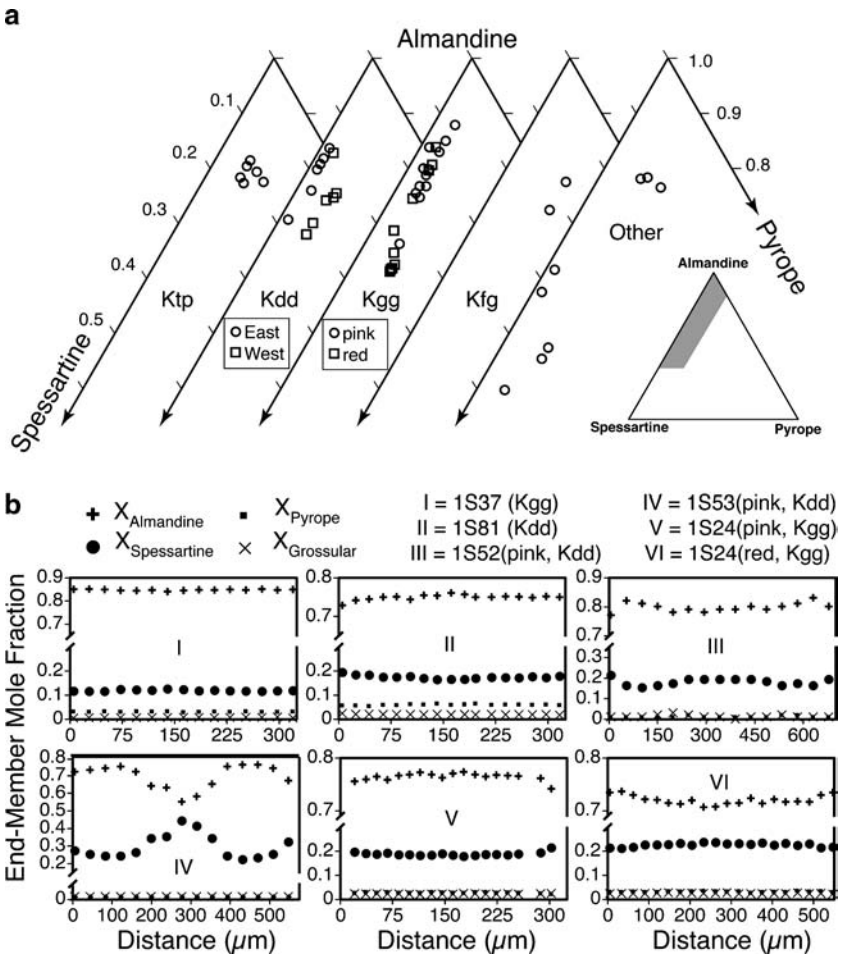

Fig. 7 Magmatic garnet cation composition. **a** Ternary diagrams with relative abundance of almandine, spessartine, and pyrope in garnet from several plutons. **b** Representative rim-to-rim zoning profiles through the cores of garnets from the Grant Grove (1S24, 1S37) and Dinkey Dome (1S52, 1S53, 1S81) plutons. In profiles, 0 distance = rim, max distance = other rim of crystal. Note *breaks* in the *y*-axis. *Ktp* Tharps Peak; *Kdd* Dinkey Dome; *Kgg* Grant Grove; *Kfg* Fine Gold; *Other* Rawson Creek, Cactus Point, Snow Corral Meadow, Smith Grade

($n = 9$), not including the 25.9‰ value obtained from a quartzite composed of marine chert fragments (Fig. 8a; Table 3). Overall, the δ^{18}O(WR) values for the ophiolitic rocks are similar to those reported for altered basalts at Kuroko, Japan (6.7 ± 1.3‰, Green et al. 1983), and overlap with some values measured in altered upper ocean crust (Muehlenbachs 1998).

Granitoids

Whole rocks

Values of δ^{18}O(WR) measured in granitic rocks (Table 4) are highly variable, but generally indicative of supracrustal input. For granites, δ^{18}O(WR) range from 9.2 to 13.0‰ and averages 10.5 ± 1.0‰ ($n = 32$), not including the Rawson Creek leucogranite, which is hydrothermally altered (δ^{18}O(WR) = 5.3‰). The δ^{18}O(WR) values of these granitoids overlap, but are generally higher than metaluminous granitoids in the central SNB (7–10‰, Masi et al. 1981; Lackey et al. 2001, 2003, 2005), and are similar to values reported for many other peraluminous plutons (Taylor and Sheppard 1986; Chappell and White 1992). Three diorite bodies associated with peraluminous plutons were analyzed for δ^{18}O(WR) and found to have values that are considerably higher than mantle-derived magmas (8.4–9.4‰, Table 3).

Minerals

In granitoids, quartz, zircon, garnet, and other accessory minerals were analyzed for δ^{18}O as their abundance allowed (Table 4). Figure 9 presents "δ–δ" plots for various mineral pairs; isotherms on the plots are calculated from published fractionation factors (Appendix 1). We note that the fractionation factors between garnet and other minerals can have considerable variability due to changing cation chemistry in garnet, especially in calcic garnets (Kohn and Valley 1998; Valley et al. 2003). However, the relatively restricted range of cation chemistry of garnets in this study does not appreciably affect equilibrium fractionation. Appendix 1 discusses why the effect is negligible in almandine–spessartine rich garnet.

The ranges of values in quartz and accessory minerals are: δ^{18}O(Qtz) = 10.3–13.8‰; δ^{18}O(Grt) = 6.6–10.4‰; δ^{18}O(Zrc) = 6.7–10.0‰. Values of δ^{18}O(Grt) are similar to those previously reported for magmatic almandine (King and Valley 2001; Harangi et al. 2001). Values of δ^{18}O(Zrc) are elevated relative to values from most

Table 3 Metamorphic wallrock $\delta^{18}O$ values, Sierra Nevada, California

Sample	Rock type	$\delta^{18}O$(WR)	Sample	Rock type	$\delta^{18}O$(WR)
Kings Sequence metasediments					
3S8	Schist	13.67	1S26	Schist	16.92
3S10	Schist	15.55	1S39	Schist	14.08
3S12	Schist	17.09	3S38A	Schist	15.48
3S13	Schist	18.12	3S38B	Schist	15.94
3S16	Schist	21.80	3S39	Schist	12.22
3S17	Schist	20.38	3S40	Schist	11.90
3S18	Schist	16.57	3S44	Schist	18.08
3S20	Schist	13.32	3S46	Schist	12.27
3S21	Schist	13.22	3S50	Schist	11.14
3S22	Schist	13.62	1S42	Schist	12.52
3S30	Schist	13.40	1S46	Quartzite	13.75
3S31	Schist	11.71	1S55	Quartzite	13.03
3S32	Schist	6.64	1S57	Schist	9.57
3S33	Schist	6.42	1S61	Schist	10.05
3S35	Schist	13.84	1S76	Schist	11.78
1S22	Schist	12.79			
Kings–Kaweah ophiolite fragments and associated intrusives					
3S2	Rodingite	6.34	3S45A	Basalt	5.34
3S3	Serpentinite	8.51	3S45A	Basalt	7.52
3S4	Quartzite	25.87	3S45B	Basalt	5.17
3S14	Serpentinite	9.03	3S5	Gabbro	7.86
3S15	Basalt	6.72	3S11	Gabbro	7.34

Metamorphic garnet in 3S12 has a $\delta^{18}O$ value of 16.75‰. Values of $\delta^{18}O$(andalusite) in 1S42 and 1S61 are 11.28 and 9.61‰, respectively; $\delta^{18}O$(sillimanite) in 1S42 and 1S61 are 11.51 and 9.47‰, respectively. Values of $\delta^{18}O$(magnetite) in the Kings Sequence quartzites are 3.93‰ (1S46) and 1.59‰ (1S55). Samples 3S32 and 3S33 are hydrothermally altered as evidenced by textures and anomalously low $\delta^{18}O$ values. Ophiolite fragments are representative samples of Paleozoic melanges in the western foothills. Basalts are pillowed. Samples 3S5 and 11 are late gabbros that cross-cut ophiolitic melange. Petrographic descriptions are given in the Lackey (2005). Sample locations are given in the Electronic Supplementary Material Supplementary. All $\delta^{18}O$ whole rock (WR) values are ‰ Vienna Standard Mean Ocean Water (VSMOW)

metaluminous plutons in the central and northern SNB (Lackey et al. 2001, 2005).

Comparison of $\delta^{18}O$(Zrc) to $\delta^{18}O$(Qtz) reveals that most quartz–zircon pairs fall between isotherms for 575 and 675°C (Fig. 9a), lower apparent temperatures than are expected for magmatic temperatures (≥650°C for the peraluminous granite solidus at pressures of 0.5–4.0 kbar; Huang and Wyllie 1981). Thus, values of $\Delta^{18}O$(Qtz–Zrc) are often in disequilibrium. Similar $\Delta^{18}O$(Qtz–Zrc) disequilibrium is recognized in the Idaho batholith (King and Valley 2001) and is explained by closed system resetting of $\delta^{18}O$(Qtz) during post-magmatic cooling. The relatively fast rate of oxygen diffusion in quartz (Farver and Yund 1991) leads to subsolidus closure temperatures (Dodson 1973). For typical cooling rates (50°C/myear) in the SNB, calculated closure temperatures for quartz grains with radii of 1 mm are 505°C. Such low closure temperatures mean that quartz would continue to exchange oxygen well below granite solidus temperatures. Thus, $\delta^{18}O$(Qtz) in the Sierra Nevada was reset from magmatic values; measured $\Delta^{18}O$(Qtz–Zrc) values confirm such resetting occurred and that it was widespread.

Quartz-garnet fractionations, $\Delta^{18}O$(Qtz–Grt), are also not in equilibrium (Fig. 9b), consistent with closed system resetting in quartz. In the Grant Grove pluton, a subset of aluminosilcate-bearing samples from the margin of the pluton (Fig. 9b) have large (>2‰) $\Delta^{18}O$(Qtz–Grt) values that cannot be explained solely by

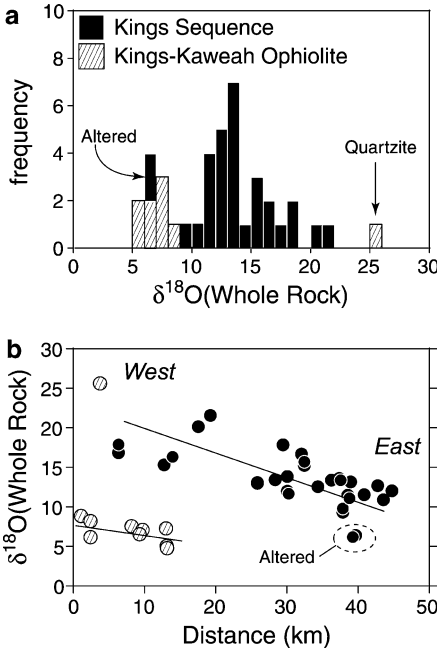

Fig. 8 Histogram of $\delta^{18}O$(WR) in metamorphic wallrocks. **a** Unaltered Kings Sequence biotite schists values are all higher than Kings–Kaweah ophiolitic rocks, except for one quartzite. **b** Regionally, the $\delta^{18}O$ of the Kings Sequence decreases from west-to-east due to the relative abundance of high-$\delta^{18}O$ chert-derived quartz in biotite schists decreases and the abundance of lower-$\delta^{18}O$ quartz derived from igneous and metamorphic rocks increases. Transect location is shown in Fig. 2

Table 4 Oxygen isotope ratios of peraluminous granitoids and related diorites, Sierra Nevada, California

Sample	Location	$\delta^{18}O$ (Qtz)	$\delta^{18}O$ (WR)	$\delta^{18}O$ (*Grt*)-I	$\delta^{18}O$ (*Grt*)-II	$\delta^{18}O$ (Zrc)	$\delta^{18}O$ Other
Peraluminous granites, granodiorites, and trondhjemites							
1S13	Grant Grove	11.71	–	7.62	–	–	
1S14	Grant Grove	11.05	–	–	–	–	
1S15	Grant Grove	11.17	–	7.61	–	–	
1S17	Grant Grove	11.31	–	7.59	7.62	–	
1S18	Grant Grove	11.14	–	7.86	–	7.87	
1S19	Grant Grove	11.43	–	7.90	–	8.29	
1S20	Grant Grove	11.15	–	7.62	–	8.02	
1S21	Grant Grove	11.31	–	7.69	–	8.29	
1S23	Grant Grove	11.51	10.56	7.81	7.93	7.86	
1S24	Grant Grove	11.52	10.38	7.44	7.83	8.03	
1S27	Grant Grove	13.36	12.84	7.56	7.91	8.97	Sill (10.68)
1S28	Grant Grove	12.98	12.47	7.76	8.89	8.44	Ghn (8.10)
1S29	Grant Grove	12.83	12.05	7.85	8.78	8.51	And (10.00)
1S30	Grant Grove	11.23	9.94	–	–	7.97	
1S31	Grant Grove	11.84	10.69	8.08	–	–	
1S32	Grant Grove	11.58	–	8.09	–	–	
1S33	Grant Grove	11.48	10.90	7.94	7.95	–	
1S34	Grant Grove	12.01	–	7.76	7.94	–	
1S35	Grant Grove	11.81	10.81	7.97	8.07	–	
1S36	Grant Grove	12.07	11.23	7.92	7.92	–	Sill (9.78); Ghn (7.35)
1S37	Grant Grove	13.80	12.97	8.22	8.80	–	Sill (11.14); Ghn (8.43)
1S38	Grant Grove	13.75	–	8.12	8.97	–	
3S41	Dinkey Dome	11.98	11.21	7.95	8.06	–	Sill (9.89)
3S42	Dinkey Dome	14.03	12.79	7.98	8.47	–	Sill (11.54); Mt (3.03)
3S43	Dinkey Dome	13.91	12.23	8.10	9.00	–	Sill (11.02); Ghn (9.52)
1S51	Dinkey Dome	10.83	9.71	7.09	–	7.76	
1S52	Dinkey Dome	11.01	9.80	6.96	–	7.51	
1S53	Dinkey Dome	10.79	9.57	7.06	–	7.53	And (8.49)
1S54	Dinkey Dome	11.03	9.90	7.21	–	7.81	And (8.46); Sill (8.34)
1S58	Dinkey Dome	10.86	9.90	7.62	–	7.77	
1S77	Dinkey Dome	11.3	9.81	6.99	–	7.63	
1S79	Dinkey Dome	10.82	9.96	7.73	–	7.67	
1S80	Dinkey Dome	11.33	10.30	7.77	–	7.72	
1S81	Dinkey Dome	10.65	9.79	7.56	–	7.76	
1S82	Dinkey Dome	11.01	9.79	7.90	–	7.73	
3S51	Dinkey Dome	11.20	10.06	–	–	8.02	Ttn2 (6.06)
1S1	Tharps Peak	11.13	9.97	7.85	7.90	7.93	
1S2	Tharps Peak	11.20	9.83	7.75	–	7.64	
1S3	Tharps Peak	11.13	10.03	7.67	7.65	7.89	
1S4	Tharps Peak	11.44	11.03	8.44	–	8.25	
1SG04	Smith Grade	13.04	11.87	9.80	10.35	8.65	
1SG05	Smith Grade	13.19	–	10.55	–	–	
1SG06	Smith Grade	12.76	–	9.54	–	–	
1S92	Ward Mountain	12.34	11.17	8.04	–	6.70	
1S93	Ward Mountain	11.40	9.91	–	–	8.10	
1S95	Hensley Lake	11.75	10.50	8.41	8.47	8.68	
1S96	Hensley Lake	11.80	10.38	8.39	–	8.72	
1S5	Cactus Point	10.28	9.19	6.74	6.77	7.15	
1S67	Snow Corral	10.64	9.54	8.65	–	7.50	Ttn1 (5.30); Ttn2 (4.81)
1S128	Rawson Creek	10.72	5.27	7.09	6.55	7.89	Ttn2 (3.84)
Associated diorites							
3S27	Cactus Point	–	9.36	–	–	8.25	Ttn1 (7.65); Ttn2 (7.35)
3S34	Grant Grove	11.79	8.40			7.53	Ttn2 (5.49)
3S48	Dinkey Dome	11.59	8.59	–	–	7.54	

Sample lithologies as given in Table 1. Sample locations are given in the Electronic Supplementary Material Supplementary. Grant Grove pluton, Gt-I and Gt-II are red and pink garnets, respectively. In other plutons, Garnet-I is darker-colored than Garnet-IIMineral abbreviations: *And* andalusite; *Ghn* gahnite spinel; *Grt* garnet; *Qtz* quartz; *Sill* sillimanite; *Ttn* Titanite; *1* primary, *2* secondary; *WR* whole rock powder. All $\delta^{18}O$ values are ‰, Vienna Standard Mean Ocean Water (VSMOW)

closed system resetting of quartz and indicate contamination at the margin of the pluton (see Discussion).

Magmatic sillimanite, andalusite, and spinel were analyzed for $\delta^{18}O$ from several samples (Table 4): $\delta^{18}O$(aluminosilicate) = 8.3–11.5‰; $\delta^{18}O$(spinel) = 7.4–9.5‰. Sillimanite and other aluminosilicates are estimated to have high closure temperatures for oxygen diffusion. In the case of sillimanite, 5 μm radius grains

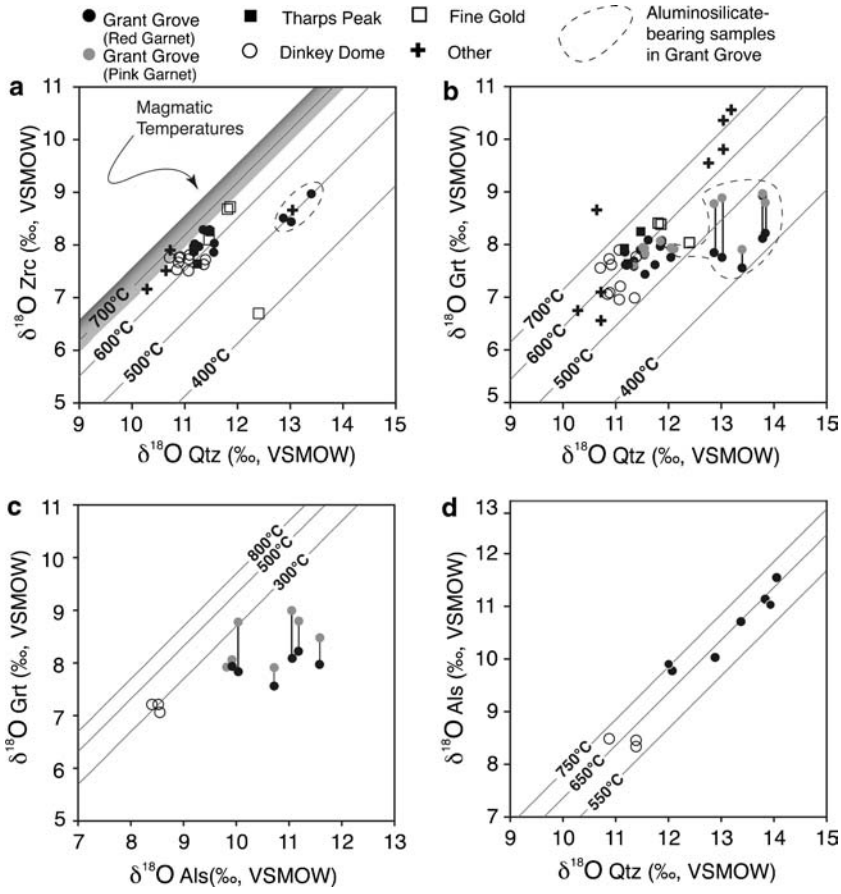

Fig. 9 δ–δ Plots of for coexisting quartz, zircon, garnet, and aluminosilicates. **a** Quartz–zircon fractionations yield apparent temperatures that are lower than magmatic temperatures and suggest δ^{18}O(Qtz) is reset. Apparent temperatures in aluminosilicate-bearing samples are lower than expected for closed system diffusional re-equilibration. **b** Quartz–garnet fractionations are more scattered than quartz–zircon, and vary considerably with different garnet populations within a sample. **c** Aluminosilicates are not equilibrated with garnet. **d** Quartz–aluminosilicate pairs in Grant Grove define a consistent isotherm

(Fig. 5b) in a rock cooling 100°/Ma will have a closure temperature (Dodson 1973) to oxygen exchange of approximately 660°C (Fortier and Giletti 1989; Ghent and Valley 1998), and thus can retain high-temperature δ^{18}O. Coexisting garnet and aluminosilicate have disequilibrium Δ^{18}O values, yielding implausible apparent temperatures (Fig. 9c). The cause of this disequilibrium appears to be different times of crystallization, which gives information about magma contamination (see Discussion). Values of Δ^{18}O(Qtz–aluminosilicate) in the Grant Grove pluton define a consistent isotherm (Fig. 9d), and thus have only been reset by 0.2–0.4‰ during closed system exchange accompanying cooling.

Diorite bodies associated with the peraluminous granitoids have high δ^{18}O(Zrc) values relative to the mantle. Values range from 7.5 to 8.3‰ (Table 4) and are anomalously high given their SiO_2 content (52 wt.%, Table 2), and are considerably elevated relative to mantle δ^{18}O(Zrc) values (5.3 ± 0.3‰; Valley et al. 1998). Further, the δ^{18}O(Zrc) values of the diorites closely match values of adjoining peraluminous plutons and therefore have high δ^{18}O relative to metaluminous granitoids in the batholith.

Pluton traverses

The spatial distribution of δ^{18}O values in the Tharps Peak, Dinkey Dome, and Grant Grove plutons provides crucial information about the contamination processes affecting each body. The δ^{18}O values from traverses (Fig. 3a–c) are plotted in Figs. 10 and 11.

At Tharps Peak, δ^{18}O values of quartz, WR, garnet, and zircon change little in the three westernmost samples (Fig. 10a), but δ^{18}O is elevated in the farthest east, within 250 m of high-δ^{18}O metasedimentary rocks of the Kaweah pendant (Fig. 10a). Average Δ^{18}O(Grt–Zrc) = 0.00 ± 0.18‰ in the pluton, indicating the two minerals are approximately equilibrated. The slightly positive Δ^{18}O(Grt–Zrc) in the easternmost sample may record modest contamination between the time when zircon and garnet crystallized.

At Dinkey Dome, values of δ^{18}O(Zrc) are very uniform across the entire pluton (7.69 ± 0.10‰, Fig. 10b). In spite of this homogeneity, values of δ^{18}O(Zrc) are less variable on the west side (7.73 ± 0.04‰) than on the east (7.65 ± 0.13‰). The δ^{18}O values of garnet mirror zircon and also show a consistent difference (δ^{18}O(Grt) = 7.71 ± 0.11‰ on west, 7.06 ± 0.10‰ on east, Fig. 10b). Average Δ^{18}O(Grt–Zrc) is −0.06 ± 0.13‰ on the west side, reflecting high temperature equilibration. On the east side, however, Δ^{18}O(Grt–Zrc) is −0.6 ± 0.13‰ indicating significant and very consistent levels of disequilibrium. Since δ^{18}O(Zrc) values are uniform across the pluton, the Δ^{18}O(Grt–Zrc) shift reflects a change in δ^{18}O only recorded by garnet (Fig. 10b), which began to crystallize after zircon. Values of δ^{18}O(Qtz) and δ^{18}O(WR) vary

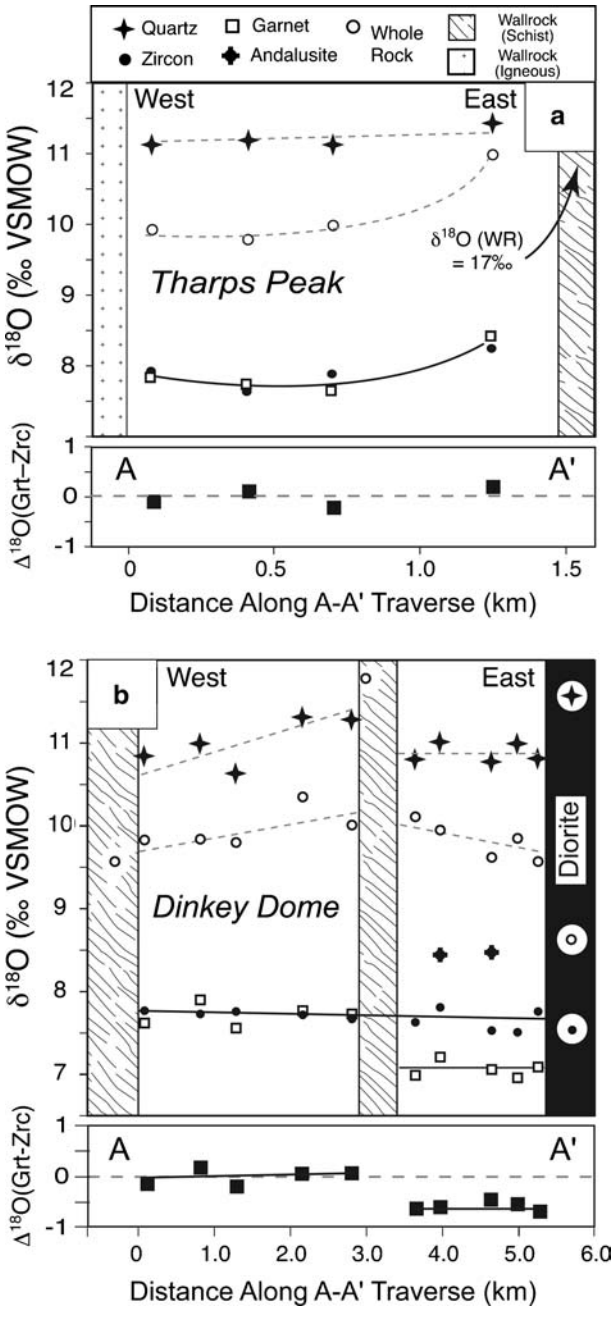

Fig. 10 Variations in $\delta^{18}O$ and $\Delta^{18}O$ across: **a** Tharps Peak pluton (A–A′ traverse; Fig. 3a). **b** Dinkey Dome pluton (A–A′ traverse, Fig. 3b)

considerably from sample to sample (Fig. 10b), and are less accurate monitors of magmatic $\delta^{18}O$ than zircon or garnet, because of post-magmatic alteration. In addition, the bimodal geochemistry at Dinkey Dome indicates that the east and west sides behaved as two independent magmatic systems, and thus are essentially different plutons.

In the Grant Grove pluton, four traverses locally record variable or no magma contamination by wallrocks. In plots of each traverse (Fig. 11), average values of $\delta^{18}O$(Zrc) and $\delta^{18}O$(WR) from garnet-absent samples in the pluton are plotted for comparison. A traverse of the garnet zone where there are no adjacent metasedimentary wallrocks (Traverse I, Figs. 3c, 11), reveals remarkable homogeneity in $\delta^{18}O$(Qtz), $\delta^{18}O$(Grt) and $\delta^{18}O$(Zrc). Furthermore, $\delta^{18}O$(Zrc) values are identical to $\delta^{18}O$(Zrc) in garnet-absent areas of the pluton. Similar $\delta^{18}O$(Zrc) systematics occur in Traverse II (Fig. 11), where a >200 m thick section of wallrock is present (Fig. 3c). Where measured, values of $\delta^{18}O$(WR) increase toward the contact with adjacent wallrocks, up to 3‰ higher than average $\delta^{18}O$(WR) of garnet-absent samples (Traverses II–IV, Fig. 11). Like $\delta^{18}O$(WR), values of $\delta^{18}O$(Qtz) also increase toward contacts. Values of $\delta^{18}O$(Zrc) and $\delta^{18}O$(Grt) record considerable disequilibrium at the margin of the pluton (Traverse II). Where $\delta^{18}O$(WR) increases, the $\Delta^{18}O$(Grt–Zrc) value is largest. Likewise, $\delta^{18}O$ values of pink versus red garnet are increasingly different from each other, with consistently higher values in pink garnet occurring near the contact of the pluton and wallrock (Traverses III and IV, Fig. 11).

Discussion

Garnet, zircon, and aluminosilicates as contamination monitors

The Idaho batholith model

King and Valley (2001) first proposed that disequilibrium $\delta^{18}O$ fractionations between garnet and zircon were systematic evidence of late-stage contamination in peraluminous magmas of the Idaho batholith. To explain the consistent pattern of $\delta^{18}O$(Grt) and $\delta^{18}O$(Zrc), the following sequence of contamination and crystallization events was proposed. First, magmas became saturated in Zr and zircon began to crystallize. Zircon was in $\delta^{18}O$ equilibrium with the host magma, and because zircon has a high closure temperature to oxygen exchange, it preserved the equilibrium $\delta^{18}O$ from the time it crystallized. The magmas were subsequently contaminated by small and variable amounts of high-$\delta^{18}O$ wallrock causing $\delta^{18}O$(magma) to increase. Despite an increase in $\delta^{18}O$(magma), the previously crystallized zircon retained its original $\delta^{18}O$. Garnet crystallization followed and $\delta^{18}O$(Grt) was equilibrated with the higher $\delta^{18}O$ contaminated magma, and thus not in equilibrium with earlier formed zircon. In contrast, major minerals like feldspar or mica that were present before contamination would have re-equilibrated their $\delta^{18}O$ values with the contaminated magma by diffusion and/or recrystallization changing their $\delta^{18}O$.

Results from Sierra Nevada plutons are presented below and indicate more variable patterns of magma evolution than in Idaho. In particular: (1) garnet, zircon, or both minerals may record contamination; (2) andalusite and sillimanite may record contamination events; (3) multiple populations of garnet may be present. An important caveat is that detailed petrography often

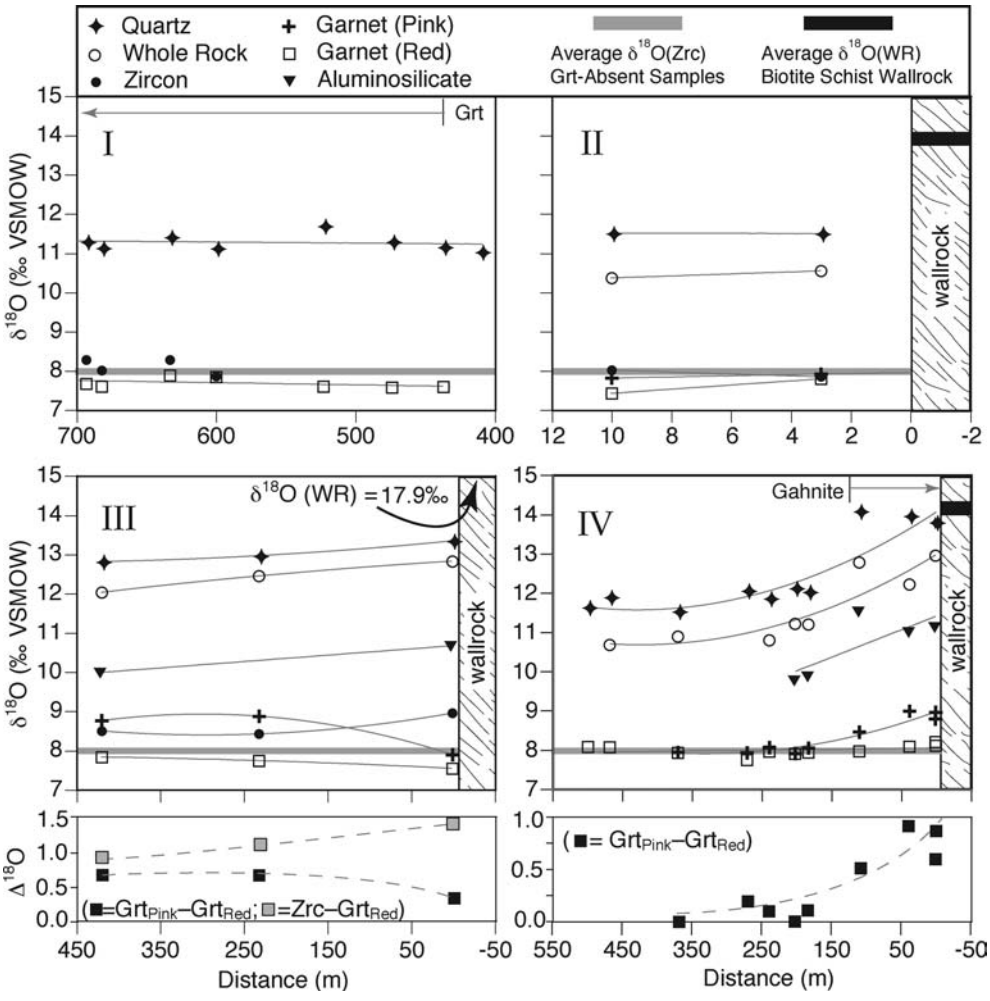

Fig. 11 Four $\delta^{18}O$ traverses (*I–IV*) in the Grant Grove pluton. Distances decrease toward the contact. Traverse numbers correspond to Fig. 3c. Average of $\delta^{18}O$(WR) and $\delta^{18}O$(Zrc) from garnet-absent parts of the pluton are shown in each traverse for comparison. Linear trendlines are fit to $\delta^{18}O$(Qtz), $\delta^{18}O$(WR) and $\delta^{18}O$(Grt) in Traverses I and II. A third-order polynomial trendline was fit to $\delta^{18}O$ (Qtz), $\delta^{18}O$(WR), $\delta^{18}O$(Grt), and $\delta^{18}O$(Zrc) where analyzed, in Traverses III and IV. Values of $\delta^{18}O$(WR) for wallrocks are indicated where analyzed

provides critical information about mineral paragenesis and the relative timing of contamination versus crystallization. Figure 12 shows $\delta^{18}O$(Zrc) versus $\delta^{18}O$(Grt) plots for the SNB plutons. Cartoons in Fig. 13 schematically depict the contamination events envisioned for the Tharps Peak, Dinkey Dome, and Grant Grove plutons.

Tharps Peak

Simple contamination and crystallization are indicated for some plutons, such as the Tharps Peak pluton (Figs. 12a, 13a). It represents a pluton that was elevated in $\delta^{18}O$ before or while garnet and zircon crystallized, potentially during a single contamination event. The array of garnet and zircon $\delta^{18}O$ values indicates high-temperature equilibrium growth of the minerals, which plot along the $\Delta^{18}O(\text{Grt–Zrc}) = 0‰$ line (Fig. 12a), and that the magma was high in $\delta^{18}O$ before either mineral crystallized (Fig. 13a). While the high $\delta^{18}O$ of the pluton is distinct from metaluminous plutons in the central Sierra, contamination is evident because even though garnet–zircon pairs are in equilibrium, they range in $\delta^{18}O$ by ~1‰. The sample with the highest $\delta^{18}O$, which is the easternmost sample (Fig. 10a), likely records local contamination while the other values may reflect the $\delta^{18}O$ of the source of this pluton (see arrow in Fig. 12a). A mass balance calculation of the amount of contamination recorded by this sample can be made assuming that the ~1‰ increases in the $\delta^{18}O$ of the sample relative to the others equal the increases in $\delta^{18}O$ of the magma due to contamination by the local wallrock. Since zircon, magma, and wallrocks contain roughly equal amounts of oxygen (~50 wt.%), the calculation of the final $\delta^{18}O$ of the magma due to contamination is as follows:

$$\delta^{18}\text{O(Magma)}_{\text{Final}} = \delta^{18}\text{O(Wallrock)}(X) + \delta^{18}\text{O(Magma)}_{\text{Initial}}(1 - X), \quad (2)$$

where X is the fraction (0–1) of wallrock contaminant. By this relationship, adding ~6 wt.% ($X = 0.06$) of the local wallrock at Tharps Peak ($\delta^{18}O$(WR)≈17‰) to this sample is sufficient to cause the local 0.5‰ increase in $\delta^{18}O$. This estimate of the percent of contamination suggests relatively limited interaction of this pluton with its wallrocks at the current level of exposure.

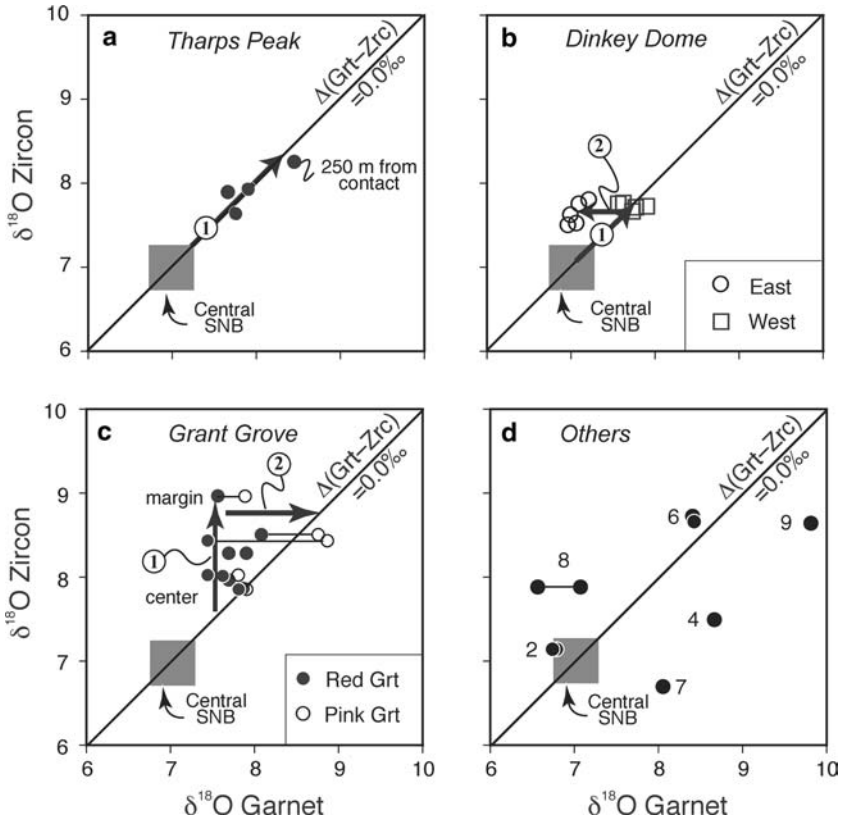

Fig. 12 Summary δ-δ plots for garnet–zircon. The equilibrium Δ^{18}O(Grt–Zrc) = 0‰ *line* is indicated as well as the average δ^{18}O(Zrc), δ^{18}O(Grt) from metaluminous granitoids of the central SNB (Lackey et al. 2001). Proposed contamination events are indicated by the *numbered arrows* and are discussed in the text and correspond to Fig. 13. **a** Tharps Peak; **b** Dinkey Dome; **c** Grant Grove; **d** other plutons. *Numbered data points* in **d** correspond to the map locations of plutons in Fig. 1

Dinkey Dome

The prominent feature of the Dinkey Dome pluton is bimodal δ^{18}O fractionation between garnet and zircon (Figs. 10b, 12b). On the west side samples record equilibrium Δ^{18}O(Grt–Zrc) values indicating that the magma was elevated in δ^{18}O before the two minerals crystallized (Fig. 12b, path 1). Despite having similar δ^{18}O(Zrc) values in both sides of the pluton, the Δ^{18}O(Grt–Zrc) value of −0.6‰ on the east side of the Dinkey Dome (Fig. 9b) records a change in magmatic condition. Either there was a decrease in magmatic δ^{18}O before garnet crystallized, or temperature dropped. Either process would cause a lower δ^{18}O(Grt) than expected on the east side, which is not in equilibrium with zircon (Fig. 12b, path 2). We discuss these two possible scenarios below.

Contamination by low δ^{18}O hydrothermally altered rock on east side of the pluton after most zircon growth could explain the disequilibrium Δ^{18}O(Grt–Zrc) values (Fig. 13b). However, only high δ^{18}O quartzite and marble are exposed in the Dinkey Creek pendant (Fig. 2b), and thus low δ^{18}O wallrock must exist at depth if this model is correct. Some low-δ^{18}O (< 0‰) hydrothermally altered volcanic (Jurassic and Cretaceous) wallrocks are known in the central and eastern SNB (Kistler 1994). At Dinkey Dome, the low δ^{18}O wallrock may have been relatively easy to melt and entirely consumed, unlike quartzite and marble in the pendant (Fig. 3b). Preferential melting of quartzofeldspathic components of metamorphic wallrock is commonly observed at deeper crustal exposures in the southern SNB (Saleeby et al. 2003).

Alternatively, garnet may have crystallized at lower temperatures than zircon on the east side. Garnet–biotite Fe–Mg thermometry by Guy (1980) yields temperature estimates of 768–700°C in the west side of the pluton and 500–600°C in the east side. Temperature estimates for the east side are well below the peraluminous granite solidus (Huang and Wyllie 1981) and presumably reflect resetting of Fe–Mg ratios in biotite. However, if garnet crystallized at *relatively* lower temperatures on the east side, larger values of Δ^{18}O(Qtz–Grt) and Δ^{18}O(Feldspar–Grt) would result. For example, using the average zircon saturation temperatures for the east side (716 ± 6°C; Table 2) as an upper temperature limit, calculated Δ^{18}O(Qtz–Zrc) values are 2.70‰. If temperature dropped to 635°C, Δ^{18}O(Qtz–Grt) is 3.29‰, which yields the observed Δ^{18}O(Zrc–Grt) of 0.59‰. Because garnet comprises less than 1% of the mode in east side rocks, crystallization in the presence of modally dominant quartz and feldspar (a much larger oxygen reservoir) would cause the 0.59‰ increase of Δ^{18}O(Qtz–Grt) to be largely accommodated by a decrease of δ^{18}O(Grt), yielding the observed Δ^{18}O(Grt–Zrc) values. While the calculated lower temperature of 635°C is largely unconstrained, it is below the peraluminous granite solidus possibly indicating subsolidus garnet growth.

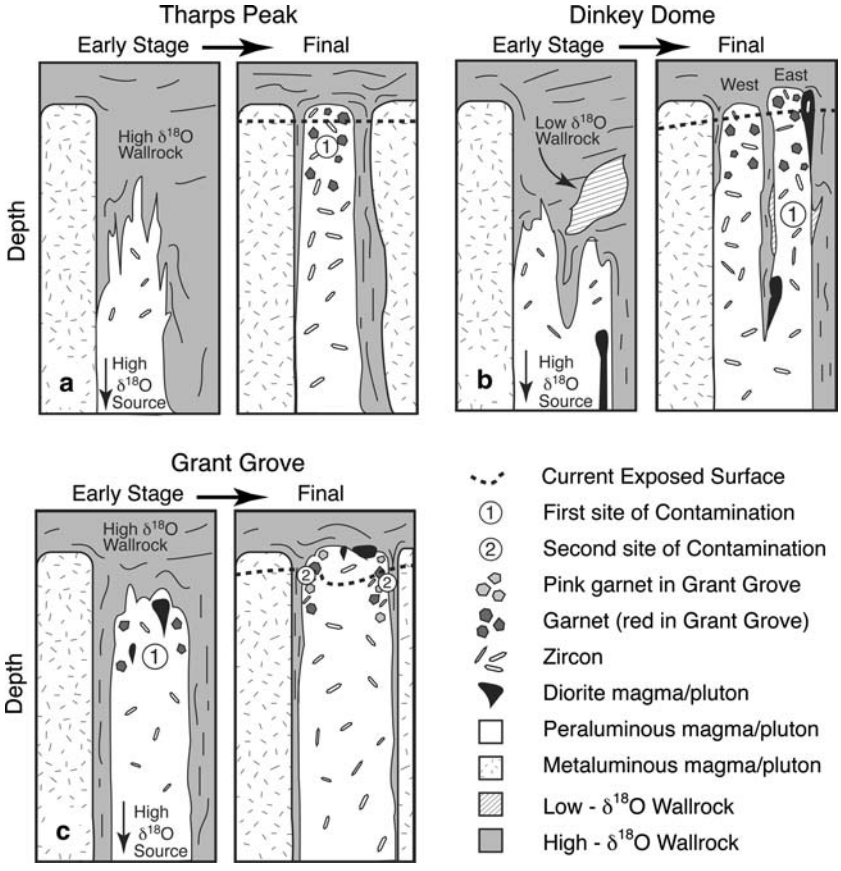

Fig. 13 Model of the petrogenesis of the **a** Tharps Peak, **b** Dinkey Dome, and **c** Grant Grove plutons. Schematic cross-sections depict mid- to upper-crustal levels of the batholith and represent contamination events revealed from $\delta^{18}O$ of zircon and garnet as shown in Fig. 12. Early and Final stages of magmatic evolution are indicated side-by-side *panels*. *Circled numbers* refer specific contamination episodes as discussed in the text. Current exposures (*dashed lines*) correlate to map surfaces in Fig. 3 and cross-sections of Tharps Peak and Dinkey Dome plutons in Fig. 10. Because the mechanisms of magma emplacement, including creation of space, are beyond the scope of this study, magma batches are shown entering the upper crust as dike-like bodies. Portrayal of plutons and adjacent wallrock with steeply dipping contacts is based on observations of such pluton–wallrock relations throughout the Sierra Nevada (cf. Saleeby et al. 2003)

Grant Grove

Garnet, zircon, and aluminosilicates record significant information about contamination in the Grant Grove pluton (Fig. 12c). Red garnet is demonstrably out of equilibrium with zircon and pink garnet in the pluton margins, but is in equilibrium with zircon further from the contact (Fig. 11, Traverses I and II). To explain the observed $\Delta^{18}O$(Grt–Zrc), an increase in $\delta^{18}O$ is suggested after crystallization of red garnet (step 1, Figs. 12c, 13). Zircon crystallization followed or was synchronous with the contamination as indicated by $\delta^{18}O$(Zrc) that increases toward the margin of the pluton (step 2, Fig. 12c). Pink garnet crystallized at the pluton margin after zircon (Fig. 13c), possibly under subsolidus conditions, and at slightly lower pressure as indicated by lower X_{grs}. The consistently smaller $\Delta^{18}O$(Qtz–Grt) values for pink garnets (Fig. 9a, b) indicate that pink garnet grew after contamination and therefore equilibrated the higher $\delta^{18}O$ magma. The best example of $\delta^{18}O$ disequilibrium between pink and red garnet is from Traverse IV (Fig. 11), where $\delta^{18}O$ of red garnet is constant across the traverse, even in samples <1 m from the contact, and matches the values of $\delta^{18}O$(Zrc) in the center of the pluton. Pink and red garnet $\delta^{18}O$ values match for samples farthest from the contact; $\delta^{18}O$ of pink garnet increases near the contact in response to localized contamination (Fig. 11). The variation in $\delta^{18}O$ between red and pink garnets, along with higher inferred crystallization pressure of red garnet based on higher X_{grs} in red garnet suggests that the magma was somewhat mobile, even in a highly differentiated state, and underwent late-stage contamination at its outer margin (Fig. 13c). In Traverse IV, the maximum amount of contamination estimated to be 16% using Eq. 2 and the differences of $\delta^{18}O$ between pink and red garnet within 50 m of the contact. Additionally, because sillimanite was the last refractory mineral to crystallize in the Grant Grove pluton, it effectively records the latest magma $\delta^{18}O$ value. Disequilibrium $\Delta^{18}O$(Qtz–Zrc) and $\Delta^{18}O$(Qtz–Grt) values indicate that garnet and zircon record earlier magma composition, whereas sillimanite records the final $\delta^{18}O$ increase of the magma.

Other examples

Other plutons studied range $\Delta^{18}O$(Grt–Zrc) values and have variable contamination histories. Samples from the Smith Grade, Ward Mountain, and Snow Corral Meadow plutons (nos. 4, 7, 9 in Fig. 12d) have positive $\Delta^{18}O$(Grt–Zrc) values (right of $\Delta = 0‰$ line), suggesting that there was contamination after zircon began to crystallize (see King and Valley 2001). These $\Delta^{18}O$(Grt–Zrc) values could not reflect variable temperature, because it would imply an increase of magma temperature of >200°C after a majority of zircon had crystallized. An increase of temperature by 200°C would result in

significant resorption of zircon, which is not observed. The Cactus Point and East Hensley Lake plutons have slightly negative Δ^{18}O(Grt–Zrc) values (Fig. 12d), suggesting that garnet crystallized at lower temperatures than zircon or was contaminated by low δ^{18}O wallrocks. The Smith Grade pluton (Fig. 12d, no. 9) has Δ^{18}O(Grt–Zrc) of 1.15‰, indicating substantial (> 20%) contamination in the margin of this pluton.

Modes of contamination and pluton assembly mechanisms

The distribution of garnet and zircon δ^{18}O within peraluminous plutons bears on whether the plutons represent single magma batches or were assembled by multiple magma batches. For example, the relative homogeneity of δ^{18}O of garnet, zircon, or both, throughout some plutons (e.g., Dinkey Dome) suggests that magmas were relatively well-mixed, allowing uniform distribution of the contaminant even through the final stages of contamination and crystallization. The Grant Grove pluton appears to have initially been well-mixed and emplaced as a single magma body. Evidence for homogeneity includes similarity of δ^{18}O(Zrc) and δ^{18}O(Grt) away from margins of the pluton and the constancy δ^{18}O of earlier forming red garnet regardless of distance to the pluton's margin (Fig. 11). Late-stage contamination in the Grant Grove pluton is clearly localized less than 200 m from contacts (e.g., pink garnet) and thus the contaminant mass was not mobile throughout the magma. In general, patterns of δ^{18}O are consistent with a model for pluton emplacement as single magma bodies rather than by incremental assembly from different magma batches.

Wholesale melting of rocks in magma sources in the lower crust can occur if there is a relatively large supply of heat from mantle-derived mafic magmas. In contrast, assimilation and fractional crystallization (AFC) processes in mid- to upper-crustal settings are limited by magma heat budgets such that melting and assimilation of wallrocks can only occur upon release of latent heat as a magma crystallizes (e.g., DePaolo 1981). In the case of the plutons studied, the relatively small amounts of contamination deduced from garnet and zircon disequilibrium are consistent with the capacity of such magmas to assimilate wallrock. The thin zone of contamination at the margin of the Grant Grove pluton suggests limited contamination at such levels in the SNB (Fig. 3c). Because these plutons are small, emplacement and crystallization of magmas as single batches would allow the most efficient melting of wallrock.

Magma sources

While the above section describes magma contamination processes in the middle and upper crust, δ^{18}O systematics for the peraluminous plutons, wallrock, and diorites, in concert with published radiogenic isotope values, yield information about original magma sources. In the SNB, δ^{18}O values indicate substantial recycling of supracrustal material, both in metaluminous and peraluminous magmas (Masi et al. 1981; Kistler 1990; Lackey et al. 2001, 2003, 2005). However, despite having high δ^{18}O, Sierran peraluminous plutons have relatively low Sr_i values. Most Sr_i values (0.705–0.708, Table 1) are lower than expected for peraluminous granitoids that contain Proterozoic sediments in their source, such as the high Sr_i (0.71–0.72) peraluminous plutons from the Cordilleran interior of the western U.S. (Miller and Barton 1990). A magma whose δ^{18}O is considerably elevated above mantle values but has relatively low Sr_i may contain a substantial component of hydrothermally altered (high δ^{18}O) ocean crust or volcanic arc sedimentary rocks, which were young at the time they were altered and thus have low Sr_i values. High δ^{18}O(Zrc), 7–9‰, metaluminous plutons in the southern and west-central Sierra Nevada that have primitive Sr, Pb, and Nd isotope ratios have been shown to contain a substantial component of such altered mantle-derived rocks (Knott 1992; Lackey et al. 2001, 2003, 2005). The least-evolved southern SNB plutons come from sources containing at least 18% of this supracrustal component (Lackey et al. 2005), which is approximately the same as that calculated for the rocks in the central SNB, based on δ^{18}O and Sr_i. We note that recognition of peraluminous magmas with primitive Sr, Nd, and Pb isotope ratios is limited (Zhou and Wang 1988; Miller et al. 1996; Gerdes et al. 2002), but that oxygen isotopes help elucidate the origins of such rocks.

Mafic–felsic magma associations

A surprising finding of this study is the high δ^{18}O(Zrc) values of diorites that match those from neighboring peraluminous plutons. While they are not highly evolved, the high δ^{18}O values of the diorites indicate they contain considerable supracrustal material. The similarity of δ^{18}O(Zrc) values between the peraluminous plutons and their neighboring diorites suggests that the two magma types are related, and potentially have the same source. Besides the mafic bodies that abut peraluminous plutons, other mafic bodies in the central Sierra also have consistently high δ^{18}O(WR) values (7.2–8.5, $n = 10$, Goldstein et al. 2005). The pervasiveness of high δ^{18}O mafic bodies in the central SNB indicates that magma source regions throughout the central Sierra included considerable amounts of supracrustal rocks.

Wallrock influence on magma contamination

Pre-batholith stratigraphy

The overall stratigraphy of prebatholithic wallrocks in the central SNB controlled the nature of contamination seen in peraluminous plutons. Basement rocks west of the PA–NA lithospheric break (Figs. 1 and 14) comprise a

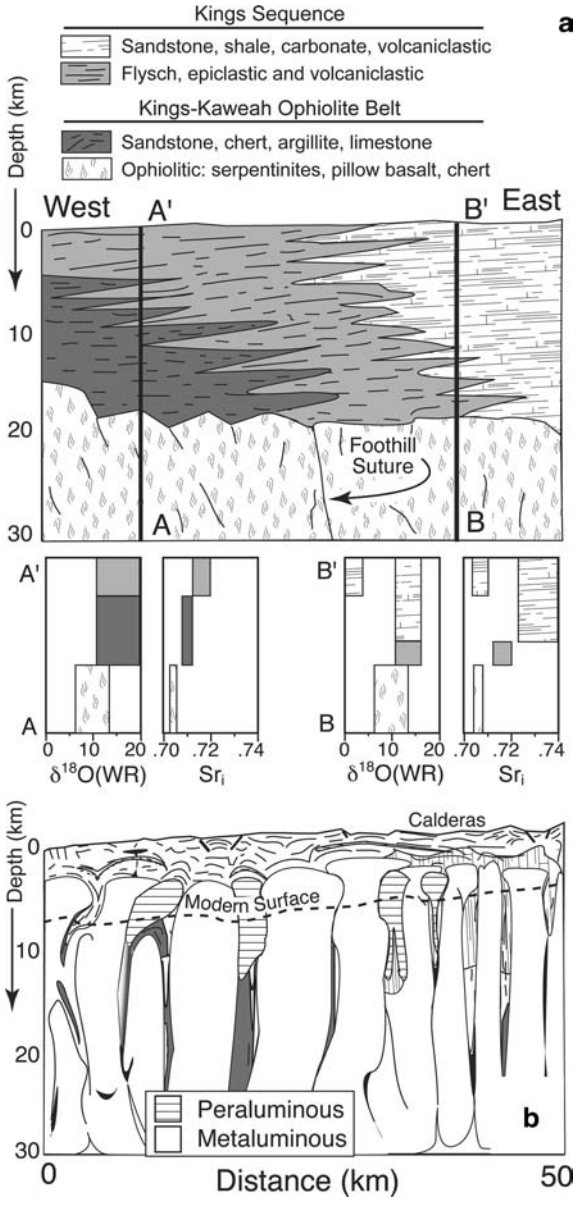

Fig. 14 Schematic cross-sections of pre- and post-batholith rocks of the west central Sierra Nevada. **a** Inferred pre-batholith wallrock configuration overlying the western Panthalassan basement in the central SNB. Isotopic "profiles" (*A–A′*, *B–B′*) illustrate highly variable isotopic stratigraphy prior to batholith formation. **b** Schematic cross-section of the eventual configuration of the western SNB showing steeply dipping pluton (metaluminous and peraluminous) contacts with interspersed screens of metamorphic wallrock. After Saleeby and Busby (1993), Saleeby et al. (2003)

complex of accreted Paleozoic abyssal lithosphere (serpentinite and pillow basalt) and associated sedimentary rocks (sandstone, chert, argillite, and limestone). These basement rocks are overlain by westward-thinning strata of lower Mesozoic submarine volcanic arc and turbiditic rocks of the Kings Sequence (Saleeby 1984, 1992; Saleeby and Busby 1993). There are facies variations in the Kings Sequence. Eastern rocks comprise shallow water sands, shales, and carbonates derived from weathering of Proterozoic rocks of the continental interior, plus scattered volcaniclastics. In the west, Paleozoic and Mesozoic flysch (epiclastic and volcaniclastic) and related olistostromes predominate (Saleeby and Busby 1993). Such lateral lithologic variation translates to the more evolved "crustal" signatures in the east than in the west (Fig. 14). A case in point, in the southern Sierra, Triassic age sections of the Kings Sequence are much more isotopically evolved ($Sr_i = 0.7430 \pm 0.012$, $\varepsilon Nd = -17.7 \pm 0.96$, $n = 4$) than adjacent Jurassic ($Sr_i = 0.7164 \pm 0.004$, $\varepsilon Nd = -9.5 \pm 0.74$, $n = 8$) pelites (Zeng 2003). This difference arises because the Jurassic rocks contain a substantial component of arc-derived sediment, which dilutes the isotopically evolved North American crustal signature typical of the Triassic rocks. Wallrocks in the Lake Kaweah pendant (Fig. 2) have isotope ratios ($Sr_i = 0.70701$, $\varepsilon Nd = -3.7$, $\delta^{18}O(WR) = 14.7‰$) that confirm this pattern (Clemens-Knott 1992), and Jurassic metavolcanic wallrocks 65 km to the northwest also have low Sr_i values (0.7040–0.7074; Kistler and Peterman 1973).

Regional $\delta^{18}O$ variations in the Kings Sequence

A notable trend of Kings Sequence biotite schists is the regular variation of $\delta^{18}O$ from west to east. When $\delta^{18}O$(WR) values are projected onto a west-to-east transect line (Figs. 2, 8), the highest values occur in western pendants and decrease eastward. Since Kings Sequence schists have similar proportions of quartz, micas, and feldspars, their variable $\delta^{18}O$ is not due to differences in mineral abundance. Instead, variation from west to east likely results from the sources of quartz in the pelites. Saleeby and Busby (1993) report a greater proportion of quartz derived from marine cherts in the western Kings Sequence. High $\delta^{18}O$ values ($> 20‰$) are typical in marine cherts (Muehlenbachs 1998). Greater proportion of marine chert in schists from western facies of the Kings Sequence best explains the regional $\delta^{18}O$ variation. Values of $\delta^{18}O$ measured on quartzite samples (Fig. 8) confirm this quartz source hypothesis. In fact, the 25.9‰ quartzite from the Kaweah ophiolite is a proxy for values of $\delta^{18}O$(Qtz) associated with oceanic rocks that were then shed into western portions of the Kings Sequence. Quartzite in the Dinkey Creek pendant (Fig. 2) has lower values ($\delta^{18}O = 13.0$–$13.6‰$) than in the west owing to greater input of igneous and metamorphic quartz. In sum, the variable $\delta^{18}O$(WR) of the Kings Sequence is a function of mixing of detrital quartz from two different sources. Moreover, the regional variation of $\delta^{18}O$(WR) in the Kings Sequence accentuates the fact that variable wallrock chemistry must be considered when quantifying local contamination in magmas.

Regional wallrock influence on magma contamination

In Fig. 14a, two hypothetical vertical crustal profiles (A–A′; B–B′) are illustrated to depict how $\delta^{18}O$ and Sr_i

values changed with depth in the prebatholithic wallrocks. As suggested by the profiles, different isotopic patterns of contamination would be expected, depending on where plutons intrude in the batholith. In the case of the western plutons like Tharps Peak, Ward Mt., and Hensley Lake (Fig. 1), the high $\delta^{18}O$, low Sr_i source values probably did not contrast markedly with wallrocks (Fig. 14a, A–A′). The Grant Grove pluton is illustrative of the pattern predicted for a pluton intruding farther east (Fig. 14a, B–B′). The interior of the Grant Grove pluton has a Sr_i value of 0.70530 (Chen and Tilton 1991); one sample at its margin is 0.70818 (Chen and Tilton 1991). Likewise, values of $\delta^{18}O$ increase at its margin (Fig. 11). Increases in both Sr_i and $\delta^{18}O$ at its margin record contamination at current crustal levels; the interior composition is close to that of its source. The Grant Grove pluton shows how peraluminous magmas emplaced into the middle and upper crust of the batholith had the isotopic signature of their sources variably overprinted depending on the kinds of wallrock they encountered. Presumably such overprinting is widespread in plutons intruding the Kings Sequence.

Conclusions

The peraluminous plutons scattered throughout the central Sierra Nevada originated from lower crustal or lithospheric mantle sources containing abundant hydrothermally altered, mantle-derived rocks. The presence of such altered rocks in the sources of peraluminous plutons explains the high $\delta^{18}O$ but relatively low $^{87}Sr/^{86}Sr$ values of peraluminous plutons in the Sierra Nevada. Magma contamination involved wallrocks of highly variable chemistry in the lower to middle crust, thus producing considerable diversity of chemistry from pluton to pluton. Whole rock and quartz $\delta^{18}O$ values on average provide general evidence for the supracrustal origins of SNB peraluminous magmas but are commonly altered by subsolidus processes. Only refractory minerals like garnet, zircon, and aluminosilicates provide a clear record of magmatic $\delta^{18}O$ variations, including evidence for progressive contamination by high-$\delta^{18}O$ supracrustal rocks. Because of differing times of crystallization among these refractory minerals, a continuous record of magmatic contamination is recorded in some cases.

Finally, we emphasize the utility of exploiting disequilibrium $\delta^{18}O$ values among refractory magmatic minerals as a monitor of evolving contamination and crystallization processes. This technique provides a powerful new means for deciphering the time-integrated effects that have long frustrated geochemical studies of magmatic systems. Results hint of considerable isotopic zoning within the refractory minerals, which can be studied by detailed single grain analysis of oxygen isotope ratios by ion microprobe. Coupling of $\delta^{18}O$ with trace element and geochronological data from refractory minerals offers exciting potential for refining contamination histories of magma systems worldwide.

Acknowledgements This study was supported by DOE 93ER14389 and NSF EAR99-02973 & 02-07340 (JWV), GSA and Sigma Xi grants (JSL), and the U.W. Department of Geology and Geophysics Weeks Fund. We thank Mike Spicuzza for assistance with stable isotope analysis, John Fournelle for assistance with the electron microprobe, and Brian Hess for making thin sections. Bruce Chappell, Elizabeth King, William Peck, Ilya Bindeman, Cory Clechenko, Aaron Cavosie, Clark Johnson, and Tom Lapen have added useful discussion and reviews of portions of this research. Jim Moore generously provided copies of unpublished maps, and Ron Kistler shared unpublished data. Laura Madsen helped in the field. David Graber assisted with sampling permits for Sequoia National Park. Calvin Miller and George Bergantz provided detailed and thoughtful journal reviews that helped us improve the overall quality of this paper.

Appendix 1

Oxygen isotope fractionation factors

Comparison of the $\delta^{18}O$ values of mineral pairs to equilibrium fractionation factors is used to test if minerals are in isotopic equilibrium. Isotopic fractionation factors are expressed as:

$$\Delta_{i-j} = \delta^{18}O\ (\text{mineral-i}) - \delta^{18}O\ (\text{mineral-j}) \approx 1000 \ln \alpha(i-j).$$

Equilibrium fractionation factors are calculated for a particular temperature using the expression:

$$\Delta(\text{mineral-i--mineral-j}) \approx A_{i-j} \times 10^6/T^2 + B_{i-j} \times 10^3/T + C_{i-j}.$$

In the expression, T is temperature (K) and A, B, and C are experimentally or empirically determined coefficients; if no coefficient is given for A, B, or C, then its value is 0.0. The following factors are used for oxygen isotopes: quartz–zircon $A = 2.64$ (Valley et al. 2003); quartz–almandine $A = 2.71$ (Valley et al. 2003); quartz–spessartine $A = 2.83$ (Lichtenstein and Hoernes 1992); quartz–grossular $A = 3.03$ (Matthews 1994); quartz–sillimanite $A = 2.25$ (Sharp 1995); and quartz–H_2O $A = 2.51$, $C = -1.46$ (Clayton et al. 1972). Combining the oxygen isotope equilibrium fractionation factors for quartz–almandine yields an almandine–aluminosilicate fractionation "A" factor of 0.46.

Garnet cation chemistry and $\delta^{18}O$

Garnet cation chemistry was compared to $\delta^{18}O$ to determine if compositional effects correlate to the variations $\Delta^{18}O$ of garnet and other minerals. For example, $\Delta^{18}O$(Qtz–Grt) can vary up to 0.8‰ in andradite and grossular-rich garnets at magmatic (> 700°C) tempera-

tures (Kohn and Valley 1998; Valley et al. 2003). Thus dependence of $\Delta^{18}O$ on garnet composition must be considered in estimates of contamination. Grossular concentrations in SNB garnets are too low ($X_{grs} < 0.04$; see Supplementary Data Table) for corresponding changes in $\Delta^{18}O$ (0–0.01‰) to be detectable by laser fluorination. Magnesium content is likewise low and would not considerably affect $\Delta^{18}O$ of garnet and other minerals. Because Mn and Fe content varies considerably in the garnets studied, the effect of these cations on $\delta^{18}O$ was evaluated. The equilibration fractionation factors for $\Delta^{18}O$(Qtz–Grt) of spessartine (Lichtenstein and Hoernes 1992) and almandine (Valley et al. 2003) are very close, therefore the effect of large compositional differences on $\Delta^{18}O$(Qtz–Grt) is small and garnet chemistry doesn't markedly affect $\Delta^{18}O$ in these rocks. For instance, at magmatic temperatures, the calculated $\Delta^{18}O$(Qtz–Grt) for the most almandine- and spessartine-rich garnets studied (1S38, $X_{Alm} = 0.87$, $X_{Sps} = 0.09$ and 1S128, $X_{Alm} = 0.39$, $X_{Sps} = 0.55$) shifts only 0.05‰. The above calculation of sensitivity to Mn and Fe content in garnet assumes a magmatic temperature and therefore the correlation of high-Mn, low-$\delta^{18}O$ garnets may result from Mn stabilizing garnet at lower temperatures (Green 1977; Miller and Stoddard 1981). Reverse Mn zoning in some garnet phenocrysts suggests this process (e.g., Fig. 7b).

References

Abdel RAF (2001) Peraluminous plutonism: nature and origin of the Moly May Leucogranite and its Coast plutonic complex granitic host-rocks, northwestern British Columbia. Can Mineral 39:1181–1196

Ague JJ, Brimhall GH (1988a) Magmatic arc asymmetry and distribution of anomalous plutonic belts in the batholiths of California: effects of assimilation, crustal thickness, and depth of crystallization. Geol Soc Am Bull 100:912–927

Ague JJ, Brimhall GH (1988b) Regional variations in bulk chemistry, mineralogy, and the compositions of mafic and accessory minerals in the batholiths of California: with Suppl Data 88–13. Geol Soc Am Bull 100: 891–911

Allan BD, Clarke DB (1981) Occurrence and origin of garnets in the South Mountain Batholith, Nova Scotia. Can Mineral 19:19–24

Bateman PC (1992) Plutonism in the central part of the Sierra Nevada Batholith, California. US Geological Survey Professional Paper 1483

Bateman PC, Wones DR (1972) Geologic map of the Huntington Lake Quadrangle, central Sierra Nevada, California. US Geological Survey Geologic Quadrangle Map GQ-0987

Brimhall GH, Lewis CJ, Danti KM, Bogatikov O, Tsvetkov A, Kolvalenko S, Gurbanov A (1992) Evidence of magmatic water saturation and development of smokey quartz in the Dinkey Dome pluton: a two-mica garnet-bearing reduced peraluminous (I-SCR) granite of the Sierra Nevada Batholith, California. Int Geol Cong Abstr 29:188

Calk LC, Dodge FC (1986) Garnet in granitoid rocks of the Sierra Nevada Batholith, California. Abstr Prog Int Mineral Assoc 14:69

Chappell BW (1999). Aluminum saturation in I- and S-type granites and the characterization of fractionated haplogranites. Lithos 46:535–551

Chappell BW, White AJR (1992) I- and S-type granites in the Lachlan fold belt. In: Brown PE, Chappell BW (eds) The second Hutton symposium on the origin of granites and related rocks, Special Paper, vol 272. Geological Society of America, Boulder, pp 1–26

Chen JH, Moore JG (1982) Uranium-lead isotopic ages from the Sierra Nevada batholith, California. J Geophys Res 87:4761–4784

Chen JH, Tilton GR (1991) Applications of lead and strontium isotopic relationships to the petrogenesis of granitoid rocks, central Sierra Nevada batholith, California. Geol Soc Am Bull 103:437–447

Clayton RN, O'Neil JR, Mayeda TK (1972) Oxygen isotope exchange between quartz and water. J Geoph Res 77:3057–3067

Clemens JD, Wall VJ (1981) Origin and crystallization of some peraluminous (S-type) granitic magmas. Can Mineral 19:111–131

Clemens-Knott D (1992) Geologic and isotopic investigations of the Early Cretaceous Sierra Nevada Batholith, Tulare County, California, and the Ivrea Zone, Northwest Italian Alps: examples of interaction between mantle-derived magma and continental crust. PhD Thesis, California Institute of Technology, 389 p

Coleman DS, Glazner AF (1997) The Sierra Crest magmatic event: rapid formation of juvenile crust during the Late Cretaceous in California. Int Geol Rev 39:768–787

Coleman DS, Frost TP, Glazner AF (1992) Evidence from the Lamarck Granodiorite for rapid Late Cretaceous crust formation in California. Science 258:1924–1926

Corfu F, Hanchar JM, Hoskin PWO, Kinny PD (2003) Atlas of zircon textures. In: Hanchar JM, Hoskin PWO (eds) Zircon, MSA reviews in mineralogy and geochemistry, vol 53. Mineralogical Society of America, Washington, pp 469–500

Coughlan RAN (1990) Studies in diffusional transport: grain boundary transport of O in feldspars, diffusion of O, strontium, and the REEs in garnet and thermal histories of granitic intrusions in south-central Maine using O isotopes. PhD Thesis, Brown University

DePaolo DJ (1981) Trace element and isotopic effects of combined wallrock assimilation and fractional crystallization. Earth Planet Sci Lett 53:189–202

Dodson MH (1973) Closure temperature in cooling geochronological and petrologic systems. Contrib Mineral Petrol 40:259–274

Ducea M (2002) Constraints on the bulk composition and root foundering rates of continental arcs: a California arc perspective. J Geophys Res 107:ECV 15.11–15.13

Farver JR, Yund RA (1991) Oxygen diffusion in quartz: dependence on temperature and water fugacity. Chem Geol 90:55–70

Fortier SM, Giletti BJ (1989) An empirical model for predicting diffusion coefficients in silicate minerals. Science 245:1481–1484

Gerdes A, Montero P, Bea F, Fershtater G, Borodina N, Osipova T, Shardakova G (2002) Peraluminous granites with mantle-like isotope compositions: The continental-type Murzinka and Dzhabyk batholiths of the east Urals. Int J Earth Sci 91:3–19

Ghent ED, Valley JW (1998) Oxygen isotope study of quartz-Al_2SiO_5 pairs from the Mica Creek area, British Columbia: Implications for the recovery of peak metamorphic temperatures. J Met Geol 16:223–230

Goldstein E (2004) Mafic rocks of Hall Mountain, Sierra Nevada batholith, California. BS Thesis, Colgate University, 80 p

Goldstein E, Peck WH, Lackey JS (2005) Mafic rocks of Hall Mountain, central Sierra Nevada batholith, California. Geol Soc Am Abstr Prog 37:47

Green TH (1977) Garnet in silicic liquids and its possible use as a P-T indicator. Contrib Mineral Petrol 65:59–67

Green GR, Ohmoto H, Date J, Takahashi T (1983) Whole-rock oxygen isotope distribution in the Fukazawa-Kosaka area, Hokuroku District, Japan, and its potential application to mineral exploration. Econ Geol Monogr 5:395–411

Guy RE (1980) The Dinkey Creek intrusive series, Huntington Lake Quadrangle, Fresno County, California. MSc Thesis, Virginia Polytechnic Institute, 125 p

Guy RE, Wones DR (1980) Petrology of the Dinkey Creek Intrusive Series, Huntington Lake Quadrangle, Fresno County, California. Geol Soc Am Abstr Prog 12:440

Harangi SZ, Downes H, Kósa L, Szabó CS, Thirlwall MF, Mason PRD, Mattey D (2001) Almandine garnet in calc-alkaline volcanic rocks of the northern Pannonian basin (eastern-central Europe): geochemistry, petrogenesis, and geodynamic implications. J Petrol 42:1813–1843

Hathaway GM (1996) Early Cretaceous peraluminous magmatism in the eastern Sierra Nevada Batholith, California. Geol Soc Am Abstr Prog 28:311

Hinke HJ (2002) Oxygen isotope evolution of the garnet-bearing Dinkey Dome pluton, Sierra Nevada, California. BS Thesis, University of Wisconsin, 48 p

Hinke HJ, Lackey JS, Valley JW (2002) Oxygen isotope record of magmatic evolution: the garnet-bearing Dinkey Dome pluton, Sierra Nevada. Geol Soc Am Abstr Prog 34:270

Huang WL, Wyllie PJ (1981) Phase relationships of S-type granite with H_2O to 35 kbar: muscovite granite from Harney Peak, South Dakota. J Geophys Res 86:10515–10529

James EW (1992) Cretaceous metamorphism and plutonism in the Santa Cruz Mountains, Salinian Block, California, and correlation with the southernmost Sierra Nevada. Geol Soc Am Bull 104:1326–1339

Jennings CW, Strand RG, Rogers T (1977) Geologic map of California. California Division of Mines and Geology 1 sheet, 1:1,000,000

King EM, Valley JW (2001) The source, magmatic contamination, and alteration of the Idaho batholith. Contrib Mineral Petrol 142:72–88

Kistler RW (1990) Two different lithosphere types in the Sierra Nevada, California. In: Anderson JL (ed) The nature and origin of Cordilleran magmatism, GSA Memoir, vol 174. Geological Society of America, Boulder, pp 271–281

Kistler RW (1994) Mesozoic intrabatholithic faulting, Sierra Nevada, California. In: Dunne G, McDougall K (eds) Mesozoic paleography of the western United States II, vol 71. Pacific Section SEPM, pp 247–262

Kistler RW, Champion DE (2001) K-Ar, $^{40}Ar/^{39}Ar$, and U-Pb mineral ages, and strontium, lead, neodymium, and oxygen isotopic compositions for granitic rocks from the Salinian composite terrane, California. US Geological Survey Open File Report 01–453

Kistler RW, Peterman ZE (1973) Variations in Sr, Rb, K, Na, and Initial Sr^{87}/Sr^{86} in Mesozoic granitic rocks and intruded wall rocks in central California. Geol Soc Am Bull 84:3489–3512

Kohn MJ, Valley JW (1998) Effects of cation substitutions in garnet and pyroxene on equilibrium oxygen isotope fractionations. J Met Geol 16:625–639

Lackey JS (2005) The magmatic and alteration history of the Sierra Nevada batholith as recorded by oxygen isotope ratios of zircon, garnet, titanite, and quartz. PhD Thesis, University of Wisconsin, 344 p

Lackey JS, Valley JW, Chen JH (2001) Correlated O-Sr-Pb isotope ratios in the West-Central Sierra Nevada Batholith, California. Geol Soc Am Abstr Prog 33:295

Lackey JS, Hinke HJ, Valley JW (2002) Tracking contamination in felsic magma chambers with $\delta^{18}O$ of magmatic garnet and zircon. In: V M Goldschmidt conference: extended abstracts, Geochim Cosmochim Acta 66(Suppl1):428

Lackey JS, Valley JW, Stockli DF, House MA (2003) Magmatic processes in the central Sierra Nevada batholith: a cryptic pre-Jurassic boundary in Long Valley, California. Geol Soc Am Abstr Prog 35:92

Lackey JS, Valley JW, Saleeby JB (2005) Supracrustal input to magmas in the deep crust of Sierra Nevada batholith: evidence from high-$\delta^{18}O$ zircon. Earth Planet Sci Lett 235:315–330

Lichtenstein U, Hoernes S (1992) Oxygen isotope fractionation between grossular-spessartine garnet and water: an experimental investigation. Eur J Mineral 4:239–249

Liggett DL (1990) Geochemistry of the garnet-bearing Tharps Peak Granodiorite and its relation to other members of the Lake Kaweah Intrusive Suite, southwestern Sierra Nevada, California. In: Anderson JL (ed) The nature and origin of Cordilleran magmatism, GSA Memoir, vol 174. Geological Society of America, Boulder, pp 225–236

Masi U, O'Neil JR, Kistler RW (1981) Stable isotope systematics in Mesozoic granites of central and northern California and southwestern Oregon. Contrib Mineral Petrol 76:116–126

Matthews A (1994) Oxygen isotope geothermometers for metamorphic rocks. J Met Geol 12:211–219

Miller CF, Barton MD (1990) Phanerozoic plutonism in the Cordilleran interior, USA. Geol Soc Am Spec Pap 241:213–231

Miller CF, Stoddard EF (1981) The role of manganese in the paragenesis of magmatic garnet: an example from the Old Woman-Piute Range, California. J Geol 89:233–246

Miller JS, Glazner AF, Crowe DE (1996) Muscovite-garnet granites in the Mojave Desert: relation to crustal structure of the Cretaceous arc. Geology 24:335–338

Miller CF, Meschter MS, Mapes RW (2003) Hot and cold granites? Implications of zircon saturation temperatures and preservation of inheritance. Geology 31:529–532

Moore JG, Sisson TW (1987) Preliminary geologic map of Sequoia and Kings Canyon national parks, California. US Geological Survey Open-File Report 87–0651

Muehlenbachs K (1998) The oxygen isotopic composition of the oceans, sediments and the seafloor. Chem Geol 145:263–273

Patino-Douce AE (1999) What do experiments tell us about relative contributions of crust and mantle to the origin of granitic magmas? In: Castro A, Fernandez C, Vigneresse JL (eds) Understanding granites: integrating new and classical techniques, Geological Society Special Publication, vol 168. Geological Society of London, London, pp 55–75

Patino-Douce AE, Johnston AD (1991) Phase equilibria and melt productivity in the pelitic system: implications for the origin of peraluminous granitoids and aluminous granulites. Contrib Mineral Petrol 107:202–218

Peck WH, Valley JW, Graham CM (2003) Slow oxygen diffusion rates in igneous zircons from metamorphic rocks. Am Mineral 88:1003–1014

Ross DC (1958) Igneous and metamorphic rocks of parts of Sequoia and Kings Canyon National Parks, California. California Department of Natural Resources, Division of Mines Special Report 53

Ross DC (1983) Generalized geologic map of the southern Sierra Nevada, California, showing the location of basement samples for which whole rock ^{18}O has been determined. U. S. Geological Survey Open-File Report 83–0904

Saleeby JB (1984) Tectonic significance of serpentinite mobility and ophiolitic melange. In: Ramond LA (ed) Melanges—their nature, origin and significance, Special Paper, vol 198. Geological Society of America, pp 153–168

Saleeby JB (1990) Progress in tectonic and petrogenetic studies in an exposed cross-section of young ($\sim$100 Ma) continental crust, southern Sierra Nevada, California. In: Salisbury MH, Fountain DM (eds) Exposed cross-sections of the continental crust, NATO ASI Series, vol 317. D. Reidel, Dordrecht-Boston, pp 137–158

Saleeby JB (1992) Petrotectonic and paleogeographic settings of US Cordilleran ophiolites. In: Burchfiel BC, Lipman PW, Zoback ML (eds) The Cordilleran Orogen: conterminous US: the Geology of North America, vol G-3. Geological Society of America, Boulder, pp 653–682

Saleeby JB, Busby C (1993) Paleogeographic and tectonic setting of axial and western metamorphic framework rocks of the southern Sierra Nevada, California. In: Dunne GC, McDougall K (eds) Mesozoic paleogeography of the western United States: II, vol 71. SEPM, Pacific Section, pp 197–225

Saleeby JB, Sams DB, Kistler RW (1987) U/Pb zircon, strontium, and oxygen isotopic and geochronological study of the southernmost Sierra Nevada Batholith, California. J Geophys Res 92:10443–10466

Saleeby J, Ducea M, Clemens-Knott D (2003) Production and loss of high-density batholithic root, southern Sierra Nevada, California. Tectonics 22. DOI 10.1029/2002TC001374

Schott RC, Johnson CM, O'Neil JR (2004) Late Cretaceous tectonic history of the Sierra-Salinia-Mojave arc as recorded in conglomerates of the Upper Cretaceous and Paleocene Gualala Formation, northern California. J Geophys Res 109:B02204. DOI 10.1029/2003JB002845

Schuermann HME (1938) Granatfuehrender Diorit aus der Sierra Nevada, Kalifornien. Neues Jahrb Mineral 74:225–250

Sharp ZD (1995) Oxygen isotope geochemistry of the Al_2SiO_5 polymorphs. Am J Sci 295:1058–1076

Snetsinger KG, Polkowski G (1977) Rare accessory uraninite in a Sierran granite. Am Mineral 62:587–588

Spicuzza MJ, Valley JW, McConnell VS (1998a) Oxygen isotope analysis of whole rock via laser fluorination: an air-lock approach. Geol Soc Am Abstr Prog 30:80

Spicuzza MJ, Valley JW, Kohn MJ, Girard JP, Fouillac AM (1998b) The rapid heating, defocused beam technique: a CO_2-laser-based method for highly precise and accurate determination of $\delta^{18}O$ values of quartz. Chem Geol 144:195–203

Stern TW, Bateman PC, Morgan BA, Newell MF, Peck DL (1981) Isotopic U-Pb ages of zircon from the granitoids of the central Sierra Nevada, California. US Geological Survey Professional Paper 1185, p 17

Taylor HP, Sheppard SMF (1986) Igneous rocks I: processes of isotopic fractionation and isotope systematics. In: Valley JW, Taylor HP Jr, O'Neil JR (eds) Stable isotopes in high temperature geological processes, Reviews in Mineralogy, vol 16. Mineralogical Society of America, Washington, pp 227–271

Truschel JP (1996) Petrogenesis of the Fine Gold intrusive suite, Sierra Nevada Batholith, California. MSc Thesis, California State University, Northridge, 137 p

Valley JW (2003) Oxygen isotopes in zircon. In: Hanchar JM, Hoskin PWO (eds) Zircon, MSA Reviews in Mineralogy and Geochemistry, vol 53. Mineralogical Society of America, Washington, pp 343–385

Valley JW, Chiarenzelli JR, McLelland JM (1994) Oxygen isotope geochemistry of zircon. Earth Planet Sci Lett 126:187–206

Valley JW, Kitchen N, Kohn MJ, Niendorf CR, Spicuzza MJ (1995) UWG-2, a garnet standard for oxygen isotope ratios: strategies for high precision and accuracy with laser heating. Geochim Cosmochim Acta 59:5223–5231

Valley JW, Kinny PD, Schulze DJ, Spicuzza MJ (1998) Zircon megacrysts from kimberlite: oxygen isotope variability among mantle melts. Contrib Mineral Petrol 133:1–11

Valley JW, Bindeman IN, Peck WH (2003) Empirical calibration of oxygen isotope fractionation in zircon. Geochim Cosmochim Acta 67:3257–3266

Vielzeuf D, Veschambre M, Brunet F (2005) Oxygen isotope heterogeneities and diffusional profiles in composite metamorphic/magmatic garnets from the Pyrenees. Am Mineral 90:463–472

Watson EB, Cherniak DJ (1997) Oxygen diffusion in zircon. Earth Planet Sci Lett 148:527–544

Watson EB, Harrison TM (1983) Zircon saturation revisited: temperature and composition effects in a variety of crustal magma types. Earth Planet Sci Lett 64:295–304

Wenner JM, Coleman DS (2003) U-Pb zircon ages for high-silica granites in the central Sierra Nevada batholith: implications for crustal generation in continental arcs. Geol Soc Am Abstr Prog 35:326

Wenner JM, Coleman DS (2004) Magma mixing and Cretaceous crustal growth: geology and geochemistry of granites in the central Sierra Nevada batholith, California. Int Geol Rev 46:880–903

White AJR, Clemens JD, Holloway JR, Silver LT, Chappell BW, Wall VJ (1986) S-type granites and their probable absence in southwestern North America. Geology 14:115–118

Wones DR, Hon R, Bateman PC (1969) Depth of crystallization of a garnet-bearing quartz monzonite of the Sierra Nevada Batholith. Eos, Trans Am Geophys Union 50:329

Zen EA (1988) Phase relations of peraluminous granitic rocks and their petrogenetic implications. Ann Rev Earth Planet Sci 16:21–51

Zeng L (2003) Non-modal partial melting of metasedimentary pendants in the southern Sierra Nevada and implications for the deep origin of within-pluton isotopic heterogeneity. PhD Thesis, California Institute of Technology, 220 p

Zhou X, Wang D (1988) The peraluminous granodiorites with low initial Sr-87/Sr-86 ratio and their genesis in southern Anhui, China. Acta Petrol Sinica 1988:36–44